Stochastic Environmental Research and Risk Assessment (2026) 40:50
https://doi.org/10.1007/s00477-026-03176-4

ORIGINAL PAPER

Multifractal characterization of meteorological droughts in Türkiye's mediterranean region using visibility graph approaches

Oguz Simsek[1] · Utku Zeybekoglu[2] · Thomas Plocoste[3] · S. Adarsh[4]

Received: 14 September 2025 / Accepted: 10 January 2026 / Published online: 13 February 2026

Abstract

This study introduces a novel framework based on visibility graph (VG) and its upside-down variant (UDVG) to assess the multifractal structure of meteorological droughts in Türkiye's Mediterranean region. Using the Standardized Precipitation Index (SPI) and Standardized Precipitation Evapotranspiration Index (SPEI) from 24 stations (1970–2022), we examined drought dynamics across time scales ranging from 1 to 24 months. The analysis shows that except for a few one-month cases, drought indices exhibit predominantly stochastic rather than chaotic behaviour, validating the use of multifractal tools. VG and UDVG approaches were then applied to 3-, 6- and 12-month series, and multifractal spectra were computed via the sandbox and Chhabra–Jensen methods. Results indicate that SPEI consistently displays stronger multifractality than SPI, confirming the added role of evapotranspiration in drought variability. The UDVG framework reduced the multifractal spread ($\Delta Dq = D_0 - D_2$) by ~30% compared to VG (mean $\Delta Dq = 0.49$ vs. 0.72), highlighting its sensitivity to low-amplitude, persistent droughts. In contrast, VG emphasises high-magnitude wet–dry fluctuations. This dual-network approach therefore provides complementary perspectives: VG is better suited to identifying extreme wet conditions, while UDVG can capture low amplitude fluctuations, which are cautionary sign leading to long term drought and its small changes can be early indicators of drought disasters. Overall, the proposed VG/UDVG-based multifractal framework provides novel insights into drought complexity and has the potential to support the development of early warning systems and adaptation strategies in Mediterranean-type climates.

Keywords Drought · Precipitation · Evapotranspiration · Multifractals · Visibility graph

1 Introduction

Accurate forecasting of hydro-climatic processes is essential for proper water management and disaster management. Drought is a complex and creeping disaster often manifested by the scarcity of rainfall, which brings considerable damage to the water balance and crop cultivation (Thomas et al. 2015). Understanding the drought characteristics is essential for effective forecasting and subsequent preparedness against disasters. For effective management of droughts, the events were classified as meteorological, agricultural, hydrological and socio-economic (Mishra and Singh 2010). Numerous indices have been developed to characterize water storage stress across different terrestrial compartments (Svoboda and Fuchs 2016). A drought event is typically identified when one or more indicators fall below a defined threshold for a sustained period (Pachore et al. 2024). For the quantification of the drought events, numerous indices were proposed considering dominant variables influencing drought (Zargar et al. 2011). In a hydrological context, meteorological drought is generally considered as the initial or primary form of drought, while it may adversely influence the soil-moisture, streamflow, groundwater and eventually affect the agricultural production and socio-economic balance. The standardized precipitation index (SPI)

✉ S. Adarsh
adarsh_lce@yahoo.co.in

1 Faculty of Engineering, Civil Engineering Department, Harran University, 63050 Sanliurfa, Turkey

2 Boyabat Vocational School of Higher Education, Construction Department, Sinop University, 57200 Sinop, Turkey

3 KaruSphere Laboratory, Department of Research in Geoscience, Les Abymes 97139, Guadeloupe, FWI, France

4 Department of Civil Engineering, TKM College of Engineering, Kollam 691005, India

proposed by McKee et al. (1993) considering the precipitation as the sole variable, and the standardized precipitation evapotranspiration index (SPEI) proposed by Vicente Serreno et al. (2010a, b) also accounting evapotranspiration are the most popular meteorological drought indicators. The streamflow drought index (SDI), standardized runoff Index (SRI), Standardized Soil Moisture Index (SSI), Standardized groundwater Index (SGI), palmer drought severity index (PDSI) etc. are some of the indices used to represent other types of droughts referred above.

Although the drought indicators are statistical indices, their temporal evolution embodies the dynamics of hydro-climatic processes. Drought development is governed by rainfall variability, evapotranspiration, and large-scale atmospheric circulation, all of which are characterized by complex features like non-linearity, intermittency, and multiscale variability. In order to assess the complexity of such series and for revealing the underlying physical mechanisms of hydro-climatic contexts, the use of advanced mathematical tools like fractal analysis, chaotic analysis or complex network analysis is highly advisable (Rahmani and Fattahi 2021; Shamseena and Adarsh 2025). The propagation from one category of drought to another, frequency and risk analysis considering drought severity and duration, teleconnection studies, prediction models using machine learning models, etc., are some of the popular research domains in understanding the drought dynamics (Adarsh et al. 2018, 2019; Achite et al. 2024; Pachore et al. 2024; Adarsh and Janga Reddy 2019; Alkubaisi et al. 2025). The microstructure complexity analysis and fluctuation analysis of drought indices are highly warranted for developing drought prediction models and on this study, the popular meteorological drought indices SPI and SPEI are considered for analyzing the complexities in a multifractal perspective.

The complex features of many hydro-climatic series often get amplified because of changes in climate or anthropogenic interventions. Therefore, scientists are usually looking forward to alternative practices and frameworks for modelling complex time series, and fractality detection is one of the promising domains in complexity assessment (Shamseena and Adarsh 2025). The theoretical basis of fractals was mainly contributed first by Benoit Mandelbrot, who defined fractals as a rough or fragmented geometrical shape which can be divided into parts, each of which is a reduced size copy of the whole (Mandelbrot 1983, 1989). In a hydraulics perspective is well proven that the turbulent flows are often characterised by energy cascade and stochastic fluctuations (Shang and Kame 2005). In a hydrological context, the concept was formally introduced in 1950s by Harold Edwin Hurst, following his observation of the tendency of annual Nile River flows to cluster into prolonged periods of high and low discharge (Hurst 1951). The related concept of self-similarity was subsequently explored by Mandelbrot and Wallis (1969), and later formalized through the introduction of fractional Gaussian noise to describe time series exhibiting long-range dependence (Mandelbrot 1971). National Research Council (NRC 1991) further defined fractal behaviour and long memory as the statistical similarity of fluctuations across multiple temporal scales, except for a scale-dependent metric. This metric characterizing the fractality or long-memory of a series differs with the method used for calculation, viz. power law exponent that describes the distribution of the power of a series in a spectral analysis, the Hurst exponent in re-scaled range analysis or the scaling exponent in detrended fluctuation analysis (DFA) (Habib et al. 2022). It is well established that an uncorrelated time series is characterized by a Hurst exponent (H) equal to 0.5. Values of H between 0.5 and 1 indicate persistent or long-memory behaviour, whereas values between 0 and 0.5 reflect anti-persistent or short-memory dynamics (Kantelhardt et al. 2006). Moreover, the strong relationship between persistence and fractal dimension has been extensively documented, including through classical box-counting approaches (Bassingthwaighte and Raymond 1994; Rangarajan and Sant 1997, 2004; Shamseena et al. 2025). Hydrological time series exhibiting stronger long-term memory are therefore expected to display longer clustering of extreme conditions, such as floods or droughts, compared to series with weaker memory. Such variability in temporal clustering has important implications for water resource planning, drought preparedness, and flood risk management (Habib 2020).

The extension of fractals to multiple moment orders and hence to multifractals was well proven in the 1990s (Schertzer and Lovejoy 1987). Over the past three decades, many algorithms were propounded for fractal or multifractal characterization of time-series, in which, the box-counting, structure-function, sand-box, Chhabra-Jenson, double-trace moments, Fourier spectrum, extended self-similarity, wavelet transform modulus maxima etc. are some of them (Shamseena and Adarsh 2025). Peng et al. (1994) proposed the Detrended Fluctuation Analysis (DFA) for fractal characterization based on a de-trending operation. Kantelhardt et al. (2002) propounded its multifractal (MF) variant (called MFDFA) for the characterisation of the time series by describing the scaling properties using multitude of exponents. The commonality lies in power law behaviour in most of the multifractal algorithms, while the difference lies in the mathematical framework followed. The seminal contribution by Kantelhardt (2002) can be considered a landmark in the history of multifractal literature. The extension of real field problems in hydro-climatology often demands proper integration of mathematical concepts for their effective utilization for forecasting.

Many studies have analysed persistence or fractal multifractal complexity of drought indices from different parts of the Globe. Tatli (2015) evaluated the persistence of Palmer Drought Severity Index (PDSI) across Turkey using the rescaled range approach. Further, they deduced predictability index (PI), fractal dimension and autocorrelation function from H values. They found significant negative trends of PDSI across the country and H-values close to unity in the places where statistically significant trends exists. They suggested that droughts can be predictable by constructing the appropriate general climate circulation models considering climatic oscillations. Tatli and Dalfes (2020) performed a similar study for Turkey using DFA method. They reported a higher DFA scaling exponent indicate the areas of higher sensitivity to droughts and related risks. The characteristic analysis of the persistence of the PDSI across diverse climate zones showed that PI of the PDSI is relatively high in the cool-temperate and montane climate zones compared to others. Hou et al. (2018) applied MFDF analysis for the characterization of the SPI series of seven homogeneous regions of China and its sources. They have reported evident multifractality in all the regions, but its strength varies between areas. Adarsh et al. (2019) performed MFDF analysis of short-, medium- and long-term drought quantified by SPI across all the Indian meteorological subdivisions. The Hurst exponents of SPI-12 and SPI-6 drought series of all subdivisions showed long-term persistence irrespective of the climatic conditions of the region, while the short-term droughts (SPI-3) of six subdivisions displayed short-term persistence. The study reported an increase in multifractal properties of all types of drought series after climatic shift of 1976/1977 This study also finds that the Hurst exponents and degree of multifractality of all types of droughts increase with increase in aggregation timescales. da silva et al. (2022) applied MFDFA of 1, 3, 6, and 12-month accumulation periods at 133 locations across the state of Pernambuco, North East Brazil with diverse climate. Apart from findings similar to that reported by Adarsh et al. (2019) for Indian main land, H-values increase in the west-east direction indicating stronger persistence of dry/wet conditions in the coastal region than in the dry semiarid inland region. The SPI-12 indicated stronger multifractality and higher complexity in the semiarid region.

Zhan et al. (2023) applied similar study in Yellow River Basin in China, considering SPEI as the drought indicator. Drought series implied multifractality with dominancy of small fluctuations and they reported that semi-arid zone experienced stronger multifractality than semi-humid zone. Azizi and Azizi (2022) applied Higuchi algorithm to find the fractal complexity analyzed multifractality of droughts in Arizona, USA considering NDVI series. They detected a wide range of exponents for describing different types of droughts across the region. Azizi and Azizi (2024) further extended the study to deduce more intense finding on drought classifications across contiguous USA. They have found that the database of exceptional drought follows a multi-fractal pattern with a wide range of exponents, while droughts that are abnormally/rarely dry, moderate, severe, extreme exhibit a mono-fractal nature with a narrower range of exponents. Pachore et al. (2024) used the multifractal theory for assessing the propagation of meteorological drought to agricultural drought across the Indian mainland. The SPI series and standardized soil moisture index (SSMI) at 1-month scale was subjected to MFDFA and found that they reveal longer average annual drought propagation time in arid and semi-arid regions (5–6 months) than shorter propagation time in Humid regions. Rahmani and Fattahi (2024) analyzed the effect of meteorological drought on river flow patterns of Hamoon Basin in Iran using MFDFA and the cross-correlation technique. The findings revealed that when the severity and frequency of meteorological droughts augmented, the river flow time-series structure's susceptibility to substantial fluctuations reduced, the river flow exhibited stronger correlations and multifractality. Gu et al. (2024) used MFDFA upon the two agricultural drought indicators GRACE Root Zone Soil Moisture Percentile and Evaporative Demand Drought Index (EDDI) along with SPI of United States in the California and Mississippi watersheds, to evaluate the drought propagation. Spatially, the increment sequence of SPI displays pronounced dependence in almost all areas. Specifically, the changes in SPI of demonstrated persistence, California, while no such regular pattern for Mississippi data. However, the increment sequences for the agricultural drought indicators exhibited anti-persistence, indicating that future drought trends may be discontinuous.

Different types of drought indices being influenced by geographical differences, meteorological factors, external climatic drivers, irrigation strategies, and varying cropping systems. Hence the complexity of such indices will also be different along with the aggregation time scale (like 1-month, 6-month). Therefore, it becomes necessary to compare the complexity of different types of drought indices like SPI/SPEI of the same geographical setting. The traditional methods of fractal analysis often capture the high amplitude fluctuations very well. Moreover, the drought being creeping phenomena its detection of origin and transformation is quite challenging when compared with raw hydrological data series like rainfall or streamflow. It is essential to capture the low amplitude fluctuations effectively along with the high amplitude, as the low amplitude fluctuations may be a warning of prolonged drought or transformation (like meteorological to hydrological drought).

For assessing the complexity of drought more modern detrending based methods, complexity analysis has emerged after 2000 (Shamseena and Adarsh 2025) and the integration of multiple mathematical tools has emerged as a promising strategy. Complex networks, and in particular visibility graphs (VG), provide a platform to analyze spatial and temporal connections within hydro-climatic datasets (Sivakumar and Woldemeskel 2014; Deepthi and Sivakumar, 2022). Since the seminal work of Lacasa et al. (2008), VG methods have been increasingly used to characterize streamflow dynamics (Luque et al. 2009; Lacasa et al. 2012; Braga et al. 2016) and other environmental processes (Carmona-Cabezas et al. 2019; Plocoste et al. 2021a). The analogy between the visibility matrix and box-counting methods facilitates its integration with sandbox (SB) algorithms, providing a viable alternative for multifractal characterization. More recently, Plocoste et al. (2021b) proposed the upside-down visibility graph (UDVG) to capture complementary aspects of time series, particularly low-intensity fluctuations in air pollution field. As the drought indices are standardized and fluctuate around a zero mean, an effective and flexible tool capable of accounting for both sign and magnitude are required to analyze their complexity. Although this approach has been applied to air pollution and streamflow time series, its potential for analyzing standardized series remains largely unexplored (Plocoste et al. 2021b; Shamseena and Adarsh 2025). Building on this progress, the present work develops an integrated visibility graph–based multifractal (VGMF) framework for drought indices, combining VG and UDVG approaches.

The main objectives are: (i) to present an alternative framework for the multifractal description of droughts using VG and its variants; (ii) to compare multifractal properties of SPI and SPEI across diverse temporal scales; and (iii) to investigate the added value of the UDVG scheme for characterizing drought dynamics.

The remainder of this paper is organized as follows. Section 2 presents the methodology, including the visibility graph framework, the upside-down visibility graph (UDVG) approach, and the multifractal algorithms employed. Section 3 describes the study region, datasets, and drought indices (SPI and SPEI). Section 4 reports the results of stochasticity detection, multifractal analysis based on VG and UDVG, and a discussion of their implications. Section 5 provides an extended discussion of the findings, while Sect. 6 summarizes the main conclusions and highlights perspectives for future research.

2 Methodology

The VGMF framework of multifractal analysis include: (i) analysing the stochastic property by degree distribution; (ii) construct visibility matrices using VG (or its variants like UDVG); (iii) applying the SB method upon VM to get the Rényi exponent and the CJ method for developing the singularity spectra. The development of VG transform signal to network, where each entry stands as node, and links between them are made in chronological sequence. By constructing a VG representation, we aim to capture the underlying temporal dynamics and explore the influence of chronological sequences on network connections. The overall methodology followed in the study is depicted in Fig. 1.

2.1 Visibility graph (VG) algorithm

Let $\{x_i\}_{i=1}^{N}$ be a real-valued time series, where each observation x_i is associated with a temporal index i. In the Visibility Graph (VG) framework, each data point of the time series is mapped to a node of a graph, and edges between nodes are defined according to a geometrical visibility criterion.

Two nodes corresponding to data points (i, x_i) and (j, x_j), with $i < j$, are said to be mutually visible if all intermediate data points (k, x_k), such that $i < k < j$, satisfy the following condition (Lacasa et al. 2008; Ghimire et al. 2020):

$$x_k < x_i + \frac{(x_j - x_i)}{j - i}(k - i) \tag{1}$$

This inequality ensures that the straight line joining (i, x_i) and (j, x_j) is not intersected by any intermediate point of the time series, preserving a direct line-of-sight between the two nodes.

By applying this visibility criterion to all possible pairs of points in the time series, the original signal is transformed into an undirected graph characterized by an adjacency matrix $A = [a_{ij}]$, where $a_{ij} = 1$ if nodes i and j are visible, and $a_{ij} = 0$ otherwise. By construction, the adjacency matrix is symmetric and all nodes are at least connected to their immediate temporal neighbors ($a_{i,j\pm1} = 1$).

Once the visibility graph is constructed, standard network metrics can be computed. In particular, the degree k_i of a node i is defined as the number of nodes visible from it, i.e.,

$$k_i = \sum_{j=1}^{N} a_{ij} \tag{2}$$

The degree distribution $P(k)$, defined as the probability that a randomly selected node has degree k, provides valuable information on the structural properties of the graph. Previous studies have shown that time series exhibiting fractal or long-range correlated behaviour often led to scale-free

Fig. 1 Framework of the implementation of VGMF method

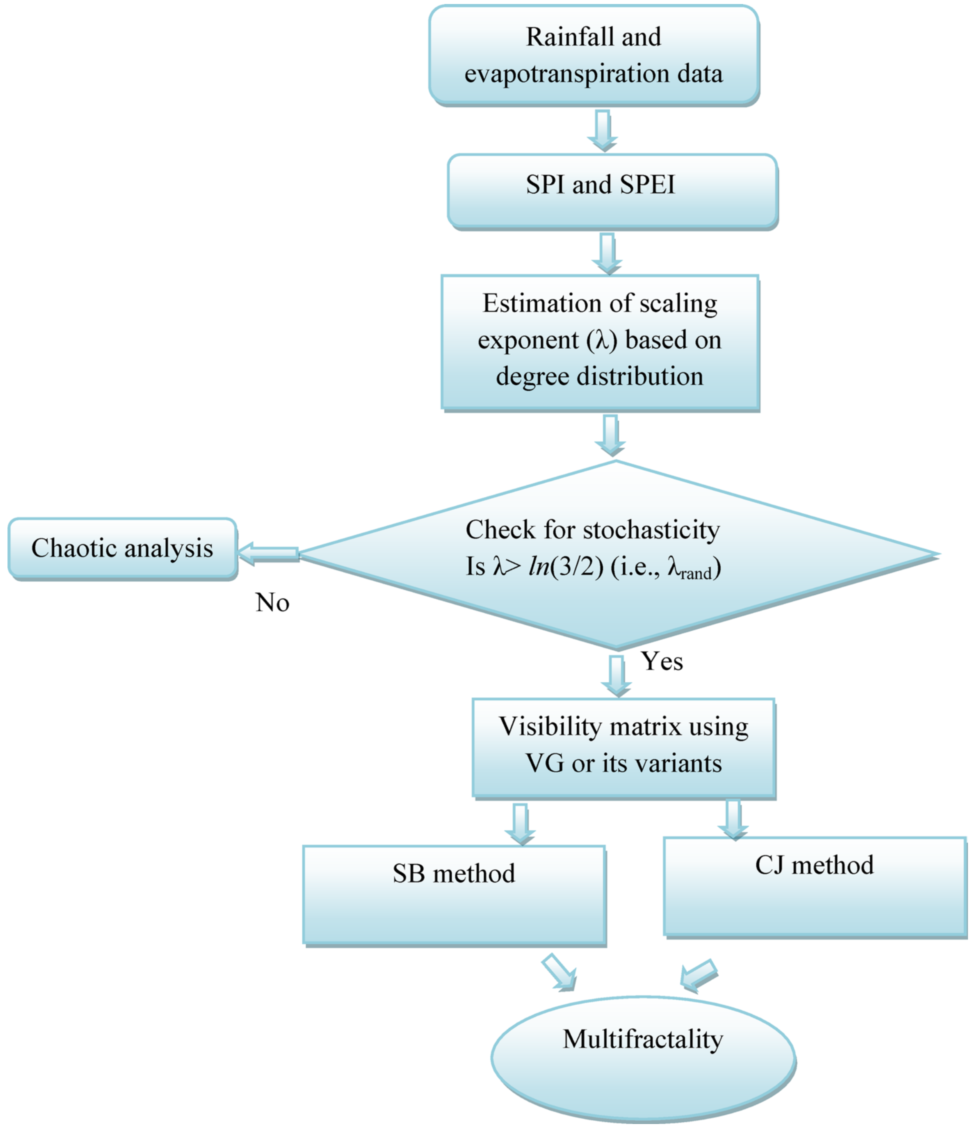

visibility graphs, where $P(k)$ follows a power-law distribution $P(k) \sim k^{-\gamma}$ (Lacasa et al. 2009; Lacasa and Toral 2010).

2.2 Sand-box (SB) algorithm

The SB method, propounded by Tél et al. (1989)and popularized by Vicsek (1990),developed from the classical box counting method, states;

$$\sum_{i=1}^{N_b} \left[\frac{M_i(\delta)}{M_o}\right]^q \propto \delta^{(q-1)D_q} \tag{3}$$

in which δ is the cell dimension, q is the moment order, i is the index of boxes, N_b is the count of boxes, $M_i(\delta)$ denotes the count of masses (particles) belongs to the i^{th} cell, and M_o is the count of masses. Previous equation can be modified as :

$$\sum_{i=1}^{N_b} [p_i(\delta)]^q \propto \delta^{(q-1)D_q} \tag{4}$$

where pi is the probability of occupancy of the ith box in the sandbox method.

Thus, the global fractal dimension (GFD) in a box-counting approach can be found out as:

$$D^{BC}{}_q = \frac{1}{q-1} \underset{\delta \to 0}{Lt} \frac{ln \sum [p(\delta)]^q}{ln(\delta)} \tag{5}$$

The SB method accounts for the count of masses occupied within a radius R, centred at the nodes. For any box with size R, $p\ (R) = M(R)\ /M0$is a probability measure of occupancy within the cell. Equation (3) can be rewritten as (De Bartolo et al. 2004):

$$\sum_{i=1}^{N_b} \left[\frac{M_i}{M0}\right]^{q-1} \left[\frac{M_i}{M0}\right] \propto R^{(q-1)D_q} \tag{6}$$

In this method, centres are chosen arbitrarily, and the mean of the masses and their q[th] moments over the centres can be estimated as $\langle [M\ (R)]^q \rangle$. Considering M_i/M_0 as a probability measure,

$$\left\langle \left[\frac{M\ (R)}{M0}\right]^{q-1} \right\rangle \propto R^{(q-1)D_q} \tag{7}$$

Then the GFD can be found out based on the expression reported in many works (Carmona-Cabezas 2019; Plocoste et al. 2021a, b) :

$$D_q = \frac{1}{q-1} \underset{R\to 0}{Lt} \frac{\ln \langle [p\ (R)]^{q-1} \rangle}{\ln(R)} \forall q \neq 1 \tag{8}$$

For $q = 1$, it D_q can be estimated as stated in Eqs. (9),

$$D_q = \underset{R\to 0}{Lt} \frac{\ln \langle p\ (R) \rangle}{\ln(R)} \tag{9}$$

The symbol$\langle \cdot \rangle$stands for the statistical mean over arbitrarily fixed centers of the SBs and detailed description of GFD formula is available in literature (Carmona-Cabezas et al. 2019).

The Renyi graph depicts the multifractal characteristics of the time series by detecting the scaling properties over diverse range of spatio-temporal scales. In general, the slope of the scaling curves gives the fractal dimension measure. As illustrated in Fig. 2, Dq for q = 0 denotes the BC dimension, D_1 indicate the information entropy and D_2 provides an idea of correlation dimension.

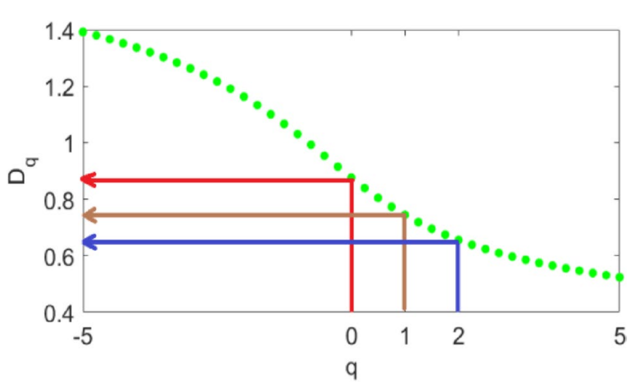

Fig. 2 Illustration of Rényi dimensions D_0, D_1, and D_2 (for q = 0, 1, 2) in a Dq vs. q plot

2.3 Upside-Down visibility graph (UDVG) method

UDVG method constructs the network from the reversed time series, offering a contrasting perspective that helps in understanding memory effects, persistent structures, and hidden asymmetries in drought behaviour. UDVG applies the VG algorithm to the inverted time series (Carmona-Cabezas et al. 2020; Plocoste et al. 2021b). For example, a SPI value of +2 becomes −2 in the inverted series. This effectively highlights the "valleys" or drought periods in the original series. Additionally, the multifractal (singularity) spectrum is helpful to describe the multifractality of the time series. We performed an analysis of the singularity spectrum $f(\alpha)$ vs. α, using the Chhabra-Jensen (CJ) method (Chhabra et al. 1989).

To further investigate low-amplitude fluctuations that are less emphasized by the standard VG, the Upside-Down Visibility Graph (UDVG) approach is employed. In this method, the VG algorithm is applied to the inverted time series, defined as $-x_i$ (Carmona-Cabezas et al. 2020; Plocoste et al. 2021b). For instance, a positive standardized index value (e.g., $SPI = +2$) becomes -2 in the inverted series. This transformation effectively highlights the minima of the original signal, which correspond to background conditions or drought periods.

By constructing the network from the reversed time series, the UDVG provides a complementary perspective to the standard VG, allowing a more detailed investigation of memory effects, persistent structures, and potential asymmetries in the temporal organization of the data. While the standard VG is primarily used to characterize high-amplitude or extreme events, the UDVG specifically targets low-amplitude dynamics and background variability.

In addition, the multifractal properties associated with the UDVG-derived measures are further explored through the analysis of the singularity spectrum. The multifractal (singularity) spectrum $f\ (\alpha)$ as a function of α is estimated using the Chhabra–Jensen method (Chhabra et al. 1989), which provides a robust characterization of the multifractality and scaling heterogeneity inherent in the time series.

2.4 Chhabra Jensen method

This method helps capture the distribution of scaling exponents (α), which characterise different intensities of α within the time series, meaning measuring the range and variation of α across the time series (Chhabra et al. 1989). This method focuses on normalised area, $\beta_i\ (q, r)$ of the original probability measure μ_i of boxes with radius r, where i is the central node and other nodes are represented as j, which can be defined as:

$$\beta_i\left(q,r\right)=\frac{\left[P_i\left(r\right)\right]^q}{\Sigma_j\left[P_j\left(r\right)\right]^q}\tag{10}$$

From this we can obtain the singularity function, $f(\alpha)$ and exponent, α as defined below:

$$f\left(\alpha\right)=\frac{\Sigma_i\beta_i\left(q,r\right)log\left[\beta_i\left(q,r\right)\right]}{logr}\tag{11}$$

$$\alpha\left(q\right)=\frac{\Sigma_i\beta_i\left(q,r\right)log\left[P_i\left(r\right)\right]}{logr}\tag{12}$$

These parameters can be obtained practically from the slopes of $\Sigma_i\beta_i\left(q,r\right)log\left[\beta_i\left(q,r\right)\right]$ over log r for $f(q)$ and the α from the slopes of $\Sigma_i\beta_i\left(q,r\right)log\left[P_i\left(r\right)\right]$ over log r. The CJ method involves plotting $f(\alpha)$ vs. α. By examining the shape and width of the spectrum, we can assess the degree of multifractality, with a wider spectrum indicating stronger variability in local scaling properties.

2.5 Standardised precipitation index (SPI)

The SPI is considered to be one of the most frequently employed drought indices (Gumus et al. 2021; Keskiner and Simsek 2024). The WMO has recommended the SPI as the main meteorological drought index that countries should use to monitor and track drought conditions (Hayes et al. 2011). McKee et al. (1993) defined SPI as the number of standard deviations by which the cumulative precipitation observed over a given time scale deviates from the long-term mean, as shown in Eq. (13).

$$SPI=\frac{X_i-\bar{X}}{\sigma}\tag{13}$$

where is the precipitation during the month i, and is the mean and standard deviation of the long-term precipitation record.

This definition enables SPI to be compared across regions with significantly different climates. Cumulative precipitation is not normally distributed; therefore, McKee et al. (1993) transformed the data to an approximately normal distribution to standardize the drought index. Thom (1958) determined that the Gamma probability distribution best fits the climate data. The density probability function for the gamma distribution may be computed using the Eq. (14).

$$G(x)=\frac{1}{\beta^\alpha\Gamma(\alpha)}x^{\alpha-1}e^{\frac{-x}{\beta}}\tag{14}$$

In this context, it is important to note that denotes the shape parameter, is the scale parameter, is the amount of precipitation, and is the gamma function. Positive SPI values indicate greater than mean precipitation, while negative values indicate less than mean precipitation. A dry period is defined as a period of time when the index is consistently negative.

2.6 Standardised precipitation evapotranspiration index (SPEI)

The SPEI was presented on the basis of the SPI by Vicente Serrano et al. (2010a). The SPEI is predicated on the principle of water balance, utilising the difference between precipitation (P) and potential evapotranspiration (PET) as the input condition to evaluate the dry and wet conditions of the area (Tirivarombo et al. 2018). A comprehensive exposition and detailed calculation methodology for the SPEI theory was provided by Vicente-Serrano et al. (2010a). The calculation of the climate-water balance is outlined as Eq. (15).

$$D_i=P_i-PET\tag{15}$$

The computation of PET is achieved through the utilisation of various methodologies, including the approaches outlined by Hargreaves (Dibike et al. 2017; Spinoni et al. 2018), Thornthwaite (Thornthwaite 1948; Wu et al. 2016; Chen and Sun 2017), and Penman–Monteith (Feng et al. 2017; Gao et al. 2017; Zhang et al. 2018) are the most methods followed for finding PET in SPEI-based studies (Singh et al. 2019; Salvacion 2021).

In this study, the PET is calculated using the Thornthwaite method (Thornthwaite 1948). In order to standardise the D series, it is necessary to employ a three-parameter distribution. It has been reported that the 3-parameter log-logistic distribution yields more optimal results for SPEI (Vicente Serrano et al., 2010a, 2010b; Tirivarombo et al. 2018; Salvacion 2021). The calculation of D and log-logistic probability density is achieved through the utilisation of the Eq. (16).

$$F(x)=\frac{\beta}{\alpha}\left(\frac{x-y}{\alpha}\right)^{\beta-1}\left(1+\left(\frac{x-y}{\alpha}\right)^{\beta}\right)^{-2}\tag{16}$$

In this study, the scale, shape and location parameters are denoted by α, β and γ, respectively. The standardisation of the cumulative distribution function (CDF) with zero mean and unit standard deviation, is then employed in order to obtain the SPEI index.

Many researchers have determined that it is more sensitive and effective than the SPI method in assessing meteorological drought. Some studies have reported that the results of the SPI and SPEI methods are generally consistent, and that the SPI method can be used instead of the SPEI method in cases of limited data availability. The use of a classification similar to the SPI method in the SPEI method enables transitions and comparisons between the two methods.

2.7 Inverse distance weighting (IDW)

Inverse Distance Weighting (IDW) is a spatial interpolation method that estimates the value at a point based on the distances of surrounding data. This method assumes that each data point receives a weight proportional to the inverse of its distance from the target point (Shepard 1968). That is, closer points have a greater influence on the estimate, while distant points have less influence. The preference for IDW in fields such as geographic information systems (GIS) and environmental modelling is due to its status as a simple and efficient method from a computational perspective (Isaaks and Srivastava 1989). However, the accuracy of IDW is contingent on the density of data points and the choice of distance function, meaning it should be applied with caution (Burrough 1986).

All analyses were performed using MATLAB. The computational framework developed in this study includes the calculation of SPI and SPEI, as well as the implementation of the visibility graph–based metrics, including degree distributions. The algorithms for VG, UDVG, and CJ multifractal analysis were adapted from the original implementations proposed by Carmona-Cabezas et al. (2020) and further improved by Plocoste et al. (2021b) to meet the specific requirements of the present study. Spatial interpolations and mapping of the derived indices were carried out using ArcGIS version 10, ensuring consistent spatial representation of drought-related metrics across the study area.

3 Datasets and study region

The study region and the spatial distribution of the stations used in the analysis of meteorological drought are presented in Fig. 3. The Mediterranean Region is located in southern Türkiye, bordered by the Mediterranean Sea to the south and the Taurus Mountains to the north. This geographical location and topographic structure give rise to the distinct characteristics of the Mediterranean climate. The Mediterranean climate is characterized by hot, dry summers and mild, wet winters, with precipitation concentrated in winter months, resulting in a pronounced water deficit during summer (Lionello et al. 2006). The elevation, latitude, and longitude information of the stations operated by the Türkiye State Meteorological Service within the study area are provided in Table 1. Station elevations range from 2 to 1344 m, with an average elevation of 277 m, resulting in considerable climatic diversity across the region. While maritime influence

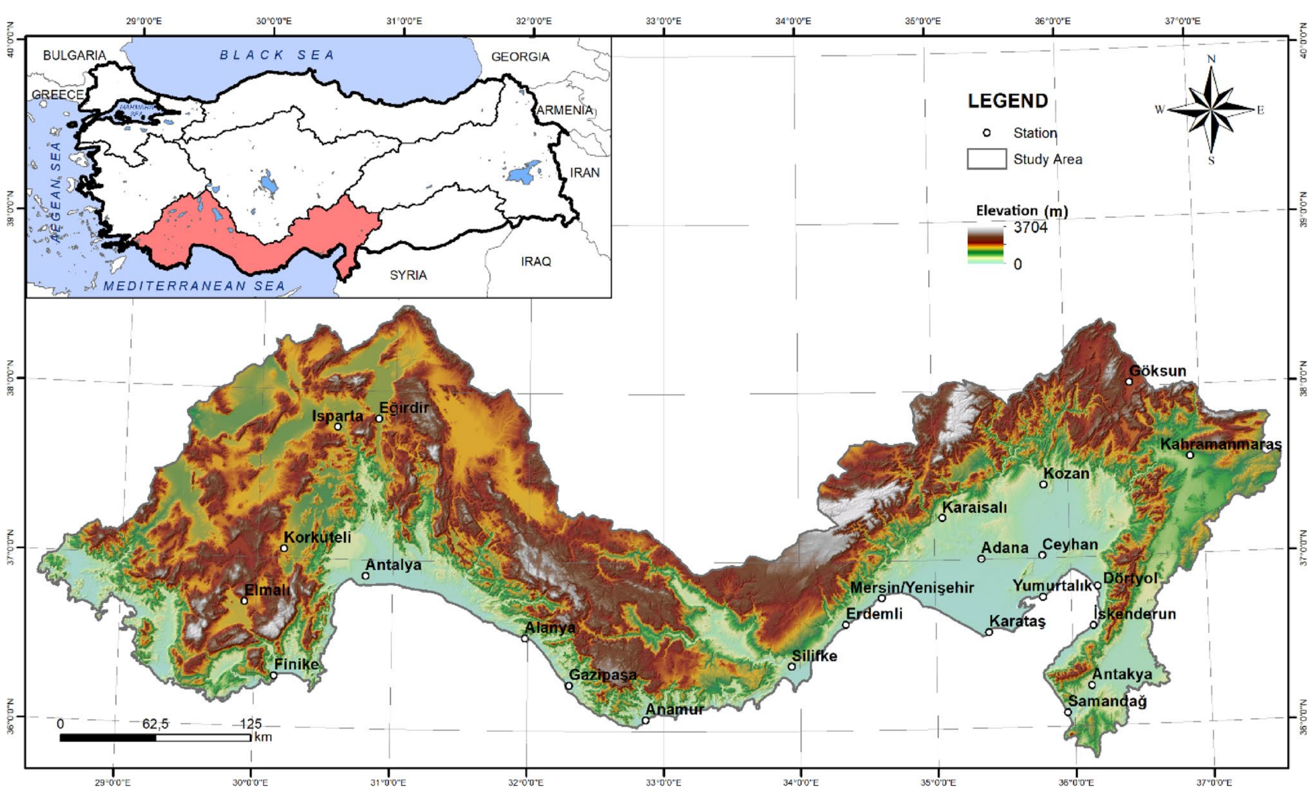

Fig. 3 Map showing the study area and stations

Table 1 Station information

Station Name	Altitude (m)	Longitude (*N*)	Latitude (E)
Adana	23	35.34	37.00
Kozan	112	35.82	37.43
Ceyhan	30	35.80	37.02
Yumurtalık	34	35.79	36.77
Karaisalı	240	35.06	37.25
Karatas	22	35.39	36.57
Gazipasa	21	32.30	36.27
Antalya	61	30.80	36.91
Elmalı	1095	29.91	36.74
Alanya	6	31.98	36.55
Finike	2	30.15	36.30
Korkuetli	1017	30.19	37.06
Dortyol	29	36.20	36.82
Antakya	104	30.80	36.24
Samadag	4	35.95	36.08
Iskenderun	4	36.16	36.59
Isparta	997	30.57	37.78
Egirdir	920	30.87	37.84
Goksun	1344	36.48	38.02
Kahramanmaras	572	36.92	37.58
Anamur	2	32.86	36.07
Erdemli	7	34.34	36.63
Mersin	7	34.60	36.78
Silifke	10	33.94	36.38

dominates the coastal areas, continental conditions become more pronounced in inland and higher-elevation areas, leading to significant spatial variations in temperature, precipitation amount, and precipitation regime. The orographic effect of the Taurus Mountains restricts the inland penetration of winter precipitation, creating a marked contrast in precipitation distribution between coastal and interior regions.

Descriptive statistics (mean, minimum, maximum, standard deviation, and kurtosis) of precipitation and average temperature data recorded over 53 years (1970–2022) are presented in Table 2. In the table, low precipitation values are indicated in red and high values in green, while high temperatures are shown in red and low temperatures in blue. The highest values of these descriptive statistics for both temperature and precipitation were identified at the Alanya, Anamur, and Antakya stations. The proximity of these stations to the coast explains their relatively higher temperatures and precipitation levels due to maritime influence. In contrast, the Elmalı, Göksun, Isparta, and Korkuteli stations exhibit lower precipitation and temperature values, which can be attributed to their higher elevations and stronger continental effects. One of the most distinctive features of the Mediterranean climate is summer drought, which, when combined with high temperatures and increased evapotranspiration, enhances the region's vulnerability to meteorological and hydrological drought (Giorgi and Lionello 2008; Vicente-Serrano et al. 2014). This condition imposes significant pressure on agricultural production, water resource management, and natural ecosystems. Although greenhouse farming and coastal tourism are widespread in the region due to high average temperatures and rising temperatures, these factors pose risks to the sustainability of these economic activities. Previous studies have identified the Mediterranean Region of Türkiye as one of the most vulnerable areas to drought, climate change, and global warming. Recent precipitation and drought events indicate an increase in both the frequency and intensity of severe dry and extreme wet periods in the region. In this context, jointly evaluating the inherent variability of the Mediterranean climate and the impacts of climate change is essential for identifying climate-related risks, ensuring the efficient and sustainable use of water resources, and determining appropriate adaptation and mitigation measures (Simsek 2021; Simsek et al. 2025; Zeybekoglu et al. 2025).

All meteorological parameters used in this study are data recorded at stations operated by the General Directorate of Meteorology of the Republic of Türkiye. The obtained data are complete and without any omissions and since these are measured values, no corrections are made before performing the study.

4 Results and discussion

4.1 Stochasticity detection

The stochastic nature of the SPI and SPEI time series was first assessed through the degree distribution (DD) using Visibility Graph (VG) approach. In line with prior studies (Carmona-Cabezas et al. 2019; Plocoste et al. 2021a), the DDs exhibited power-law characteristics, with variations in scaling exponents (λ) across stations and time scales (1–24 months). Notably, for most stations, the scaling exponent λ was found to be greater than the threshold of 0.4055—indicative of a predominantly stochastic rather than chaotic behaviour in both indices. This supports the use of complex network approaches for multifractal assessment of hydro-climatic signals. For analyzing the predictability of drought indices, firstly the stochastic fluctuations of droughts to be evaluated. The scaling exponent values are presented in Table 3. The results indicate that, except for short-term droughts at the 1-month timescale, the scaling behaviour is predominantly stochastic rather than chaotic. Overall, drought indices at the 1-month scale (SPI-1 and SPEI-1) exhibit higher complexity and a stronger tendency toward chaotic dynamics. While SPI-1 series often display chaotic behaviour, the corresponding SPEI-1 series may remain stochastic, highlighting the role of evapotranspiration in modulating short-term drought dynamics. The spatial

Table 2 Descriptive statistics for temperature and precipitation parameters

Parameter	Precipitation (mm)					Temperature (°C)				
Station	Mean	Min.	Max.	Std. Dev.	Kurts	Mean	Min.	Max.	Std. Dev.	Kurts
Adana	648.30	316.80	1176.20	196.38	0.09	19.43	18.10	20.90	0.58	0.22
Alanya	1102.13	623.90	1785.60	300.27	-0.39	19.95	18.10	22.20	1.20	-1.15
Anamur	906.71	447.10	1755.10	257.91	1.16	19.56	17.90	21.40	0.79	-0.80
Antakya	1082.76	600.00	1947.70	279.14	0.36	18.40	16.70	19.90	0.58	0.34
Antalya	1018.10	283.90	1891.80	321.19	0.01	18.77	17.10	20.30	0.79	-0.88
Ceyhan	671.57	38.20	1130.20	199.70	1.35	18.10	13.80	19.90	0.98	5.32
Dörtyol	913.44	252.00	1305.80	203.46	0.58	19.19	17.90	20.90	0.71	-0.46
Eğirdir	785.43	243.50	1404.70	209.23	1.08	12.69	10.20	14.50	0.85	-0.03
Elmalı	465.06	171.50	761.20	117.55	-0.10	13.00	10.80	14.70	0.70	0.85
Erdemli	547.24	183.70	1001.10	170.39	0.11	18.72	17.00	19.90	0.54	0.61
Finike	924.75	362.40	1553.00	261.34	0.22	19.34	17.90	21.10	0.85	-0.95
Gazipaşa	840.51	408.20	1431.30	217.49	-0.01	18.78	17.30	20.50	0.68	-0.32
Göksun	566.78	115.40	881.00	146.77	1.00	9.12	6.40	11.20	0.96	0.10
İskenderun	736.31	480.10	1009.90	124.90	-0.34	20.37	18.80	22.10	0.75	-0.57
Isparta	510.40	285.00	804.70	116.69	-0.59	12.30	10.40	14.70	0.92	0.17
Kahramanmaraş	713.06	347.20	1169.00	173.73	0.43	17.01	15.00	18.60	0.83	-0.72
Karaisalı	855.52	240.50	1429.00	245.70	-0.16	18.73	16.90	20.30	0.66	0.14
Karataş	745.92	294.00	1269.60	224.21	-0.26	19.30	17.70	20.80	0.63	-0.10
Korkuteli	364.17	94.10	589.80	94.95	0.31	12.80	11.20	14.30	0.70	-0.48
Kozan	800.80	166.00	1297.40	186.43	1.71	19.63	17.80	21.20	0.72	-0.19
Mersin	591.30	278.80	1033.70	179.05	-0.09	19.72	18.00	21.60	0.95	-1.11
Samandağ	860.28	209.10	1299.80	234.19	0.19	19.35	17.50	21.10	0.70	0.34
Silifke	557.36	300.50	1007.70	160.82	-0.10	19.74	17.80	21.70	0.82	-0.35
Yumurtalık	768.87	212.50	1334.80	218.50	-0.03	19.25	17.50	20.70	0.68	-0.38
Study Area	749.03	496.30	1086.30	146.00	-0.53	17.63	15.91	19.16	0.69	-0.30

variability of SPI and SPEI series across the Mediterranean basin is depicted in Fig.4 and Fig.5 respectively. Beyond these temporal differences, a clear spatial variability can also be observed across the Mediterranean basin (Fig. 5). Stations located along the Taurus Mountains (e.g., Göksun, Isparta, Elmalı) tend to exhibit higher scaling exponents, reflecting the influence of complex orographic effects on precipitation and drought persistence. In contrast, coastal stations such as Antalya, Alanya, and Mersin display lower values, more strongly modulated by maritime influences and Mediterranean circulation. Intermediate behaviour is observed in transitional areas, where evapotranspiration gradients amplify differences between SPI and SPEI. These spatial contrasts confirm that drought dynamics are not uniform across the region but strongly shaped by topography and climatic setting, reinforcing the added value of multifractal tools to disentangle local hydro-climatic signatures. The degree distribution (DD) plots help to confirm the existence of scaling. The sample plots for SPI/SPEI series at different scales (3, 6 and 12 months) of two stations each from three basins (Elmali, Antalya, Silifke, Adana, Ceyhan, Antakya) are presented in Supplementary information (SI) file. The exponents generated from DD plots are presented in Table S1, values of which are ranging from 1.41 to 3.58 approximately, the lowest value being for 12- month series and highest for 3-month series for majority of the cases.

Table 3 Scaling exponent of the SPI and SPEI series of the mediterranean region

Station	SPI					SPEI				
	SPI1	SPI3	SPI6	SPI12	SPI24	SPEI1	SPEI3	SPEI6	SPEI12	SPEI24
Adana	**0.3887**	0.6673	0.5744	0.5136	0.8786	**0.3594**	0.6002	0.575	0.4928	0.5516
Alanya	0.5954	0.5509	0.602	0.5187	0.5614	**0.4124**	0.5679	0.5932	0.524	0.8959
Anamur	0.4822	0.4986	0.5857	0.5988	0.499	0.4985	0.5814	0.5433	0.5229	0.5445
Antakya	**0.4084**	0.887	0.543	0.4979	0.5201	0.4527	0.6075	0.5579	0.6019	0.5269
Antalya	**0.408**	0.8847	0.5749	0.5497	0.5345	0.4632	0.5753	0.5611	0.453	0.4079
Ceyhan	**0.4042**	0.6228	0.5639	0.6312	0.5144	0.3885	0.5196	0.6136	0.6177	0.6236
Dörtyol	0.4724	0.6322	0.8181	0.8341	0.876	0.7496	0.511	0.5912	0.8654	0.8682
Eğirdir	**0.3876**	0.7404	0.8148	0.82	0.538	**0.4177**	0.5851	0.5912	1.213	0.9489
Elmalı	**0.4023**	0.8747	0.558	0.6107	0.8125	0.434	0.9412	0.9219	0.9541	0.9709
Erdemli	0.4616	0.5943	0.7678	0.8	0.5758	0.5232	0.6318	0.6314	0.8416	0.5717
Finike	**0.3925**	0.4655	0.48	0.5308	0.9548	0.4299	0.5476	0.5477	0.475	0.6528
Gazipaşa	0.8303	0.5712	1.271	0.9576	0.9127	**0.4133**	0.5266	0.993	0.5485	0.9521
Göksun	0.4128	0.567	0.8846	0.6143	0.9549	0.4232	0.5892	0.6506	0.9962	0.9795
Iskenderun	0.4953	0.5447	0.4716	0.5406	0.7283	0.4508	0.9325	0.9513	0.5415	0.9622
Isparta	0.5348	0.5832	0.6015	0.5692	0.8828	0.4551	0.5918	0.558	0.5000	0.6043
Kahramanmaraş	**0.3736**	0.508	0.5679	0.4723	0.5588	0.8539	0.9625	0.6294	0.5245	0.4737
Karaisalı	0.446	0.8137	0.5868	0.5157	0.5933	0.4997	0.9569	0.5446	0.4978	0.5623
Karataş	0.5065	0.5129	0.9294	0.8099	0.4762	0.4795	0.5761	0.6349	0.5679	0.8467
Korkuteli	0.8128	0.9117	0.6406	0.5844	0.6319	0.515	0.9027	0.6028	0.7754	0.987
Kozan	0.4041	0.5312	0.5753	0.5627	0.607	**0.393**	0.511	0.599	0.8435	0.6266
Mersin	0.4817	0.9192	0.556	0.4828	0.5901	0.4485	0.9445	0.9236	0.5995	0.6108
Samandağ	0.4738	0.977	0.5587	0.4851	0.5756	0.5151	0.5905	0.6039	0.5522	0.4557
Silfke	**0.4357**	0.9483	0.5815	0.9881	0.4931	**0.4123**	0.5999	0.6405	0.5954	0.838
Yumurtalık	**0.3954**	0.9112	0.9287	0.8571	0.6198	**0.4134**	0.9177	0.6491	0.5388	0.5479

The bold numbers imply that the corresponding drought index (SPI/SPEI) series shows chaotic behaviour

Also, SPEI possesses larger exponents than SPI of the corresponding station and scale in general, even though local climatic influences if found to destroy the pattern and deviating it from universality or generalizability. This also supports the conclusions drawn on scaling reported in earlier studies (Plocoste et al. 2021 a, b).

4.2 VG-based multifractal analysis

The SPI and SPEI series of each station, for different scales 3-month, 6-month and 12-month, are subjected to multifractal analysis in a VG frame, as these three scales represent short, moderate and long-term droughts. Also, it is worth mentioning that 1 a 1-month scale series of many stations is more of a chaotic origin and does not show stochastic fractal fluctuations. In the implementation, $R \in [R_{min}, R_{max}]$, R can be selected between 1 and N, where N *is* the total count of nodes. A larger R_{max} leads to redundancy of information while smaller R_{max} necessitate large number of boxes to cover the complete series. Researchers performed numerical exercises on this, and we noted that for a series of length between 2000 and 36,000, $R \in [1, 30]$ was found to be good enough (Plocoste et al. 2021a, b; Shamseena et al. 2025). Thus, we selected $R \in [1, 30]$ and the q-order range as [-5, 5] with step-size of 0.25 considering recommendations of past studies (Shamseena et al. 2025).

To further assess the robustness of the multifractal results, we examined the validity range of the scaling laws and the stability of the estimated exponents. Scaling behaviour was found to be consistent across moment orders within $q \in [-5, 5]$, with stable linear trends in the Rényi plots. In addition, numerical experiments confirmed that for SPI and SPEI time series longer than 600 months, the sandbox approach yields reliable estimates up to $R = 30$, beyond which redundancy effects tend to appear. Within this validity range, the multifractal exponents (D_0, D_1, D_2) remained stable across stations and temporal scales, supporting the robustness of the VG-based framework. Deviations from scaling were mostly observed at the shortest time scales (1 month), where chaotic fluctuations dominate, and at very high positive q-values, where extreme events exert disproportionate influence on the spectrum. These findings are consistent with the recommendations of Shamseena et al. (2025), who highlighted $q \in [-5, 5]$ and $R \leq 30$ as the most reliable ranges for hydro-climatic time series analysis.

Multifractal properties of the SPI and SPEI indices were quantified using Rényi dimensions (D_0, D_1, D_2) derived from the sandbox method. In line with findings from air pollution studies, a clear contrast was observed between the

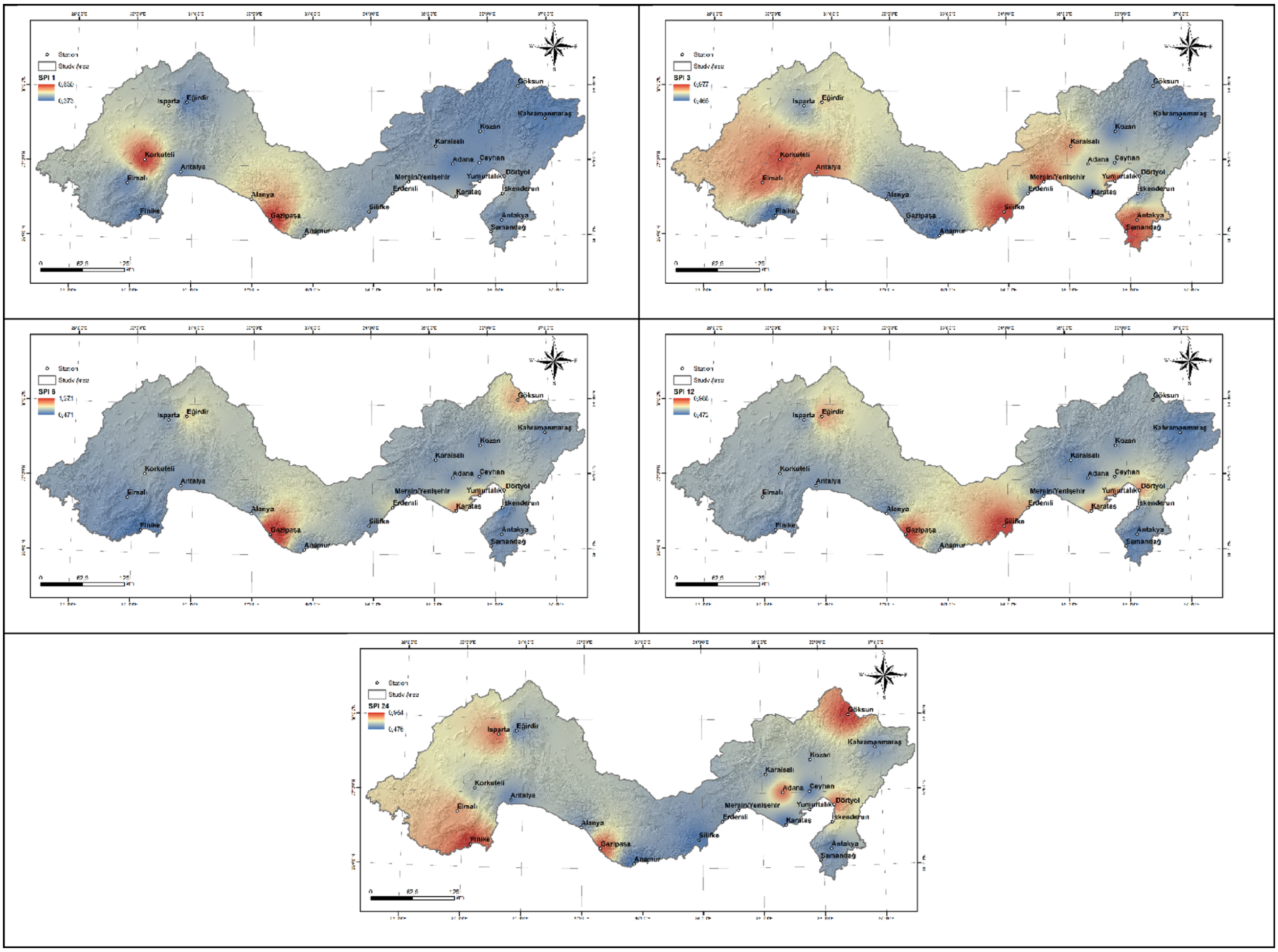

Fig. 4 Spatial variability of scaling exponents of SPI series of the Mediterranean region at different time scales (1, 3, 6, 12 and 24 months)

two graph structures. The fractal dimension exponents D_0, D_1 and D_2 were computed for each SPI and SPEI series of each station, for different time scales 3, 6 and 12 months. The multifractal degree was quantified by multifractality coefficient ($\Delta Dq = D_0 - D_2$) and plotted spatially as shown in Fig. 6 for SPI and SPEI series. In this Figure, the left panels show the results of the SPI series, while right panels show the results of the SPEI series. The SPI and SPEI time series generally exhibited higher multifractality degrees ($\Delta Dq = D_0 - D_2$), particularly at shorter time scales, suggesting stronger heterogeneity in large fluctuations—potentially linked to abrupt rainfall deficits. A comparative analysis revealed that SPEI generally exhibited more complex multifractal structures than SPI across the region. This suggests that evapotranspiration introduces additional variability, especially at longer time scales. The spatial and temporal divergence in D_0, D_1, and D_2 values between the two indices confirms the added value of SPEI in characterizing prolonged drought conditions.

The variation of the generalized dimensions Dq indicates stronger scaling heterogeneity for SPEI compared to SPI, reflecting the added influence of temperature-driven evapotranspiration on drought dynamics. Along with the coefficients of Rényi dimensions, the complementary multifractal parameters (CMPs) of the spectrum like the multifractal width, asymmetry index and Holder exponent can also provide useful insights on multifractality as referred in earlier studies (Adarsh et al. 2019). The CMPs provide additional insight into the contrasting behaviour of SPI and SPEI. Rényi dimensions of all the drought series along with the CMPs are deduced from the multifractal analysis and the values are presented in SI file. To get a broad picture of the complexity of drought, the basic statistics of the CMPs derived from VG are provided in Table 4, while similar statistics derived from UDVG are provided in SI file.

From Table 4 and Table S2-S4 in SI file, it can be noted that all the drought index considered in the series possesses positive asymmetry irrespective of scale and type (SPI/SPEI), which indicates that the multifractality of the time series is dominated by large fluctuations (high volatility events or strong trends). The drought dynamics are dominated by local high fluctuations, or a 'fine-structured' series

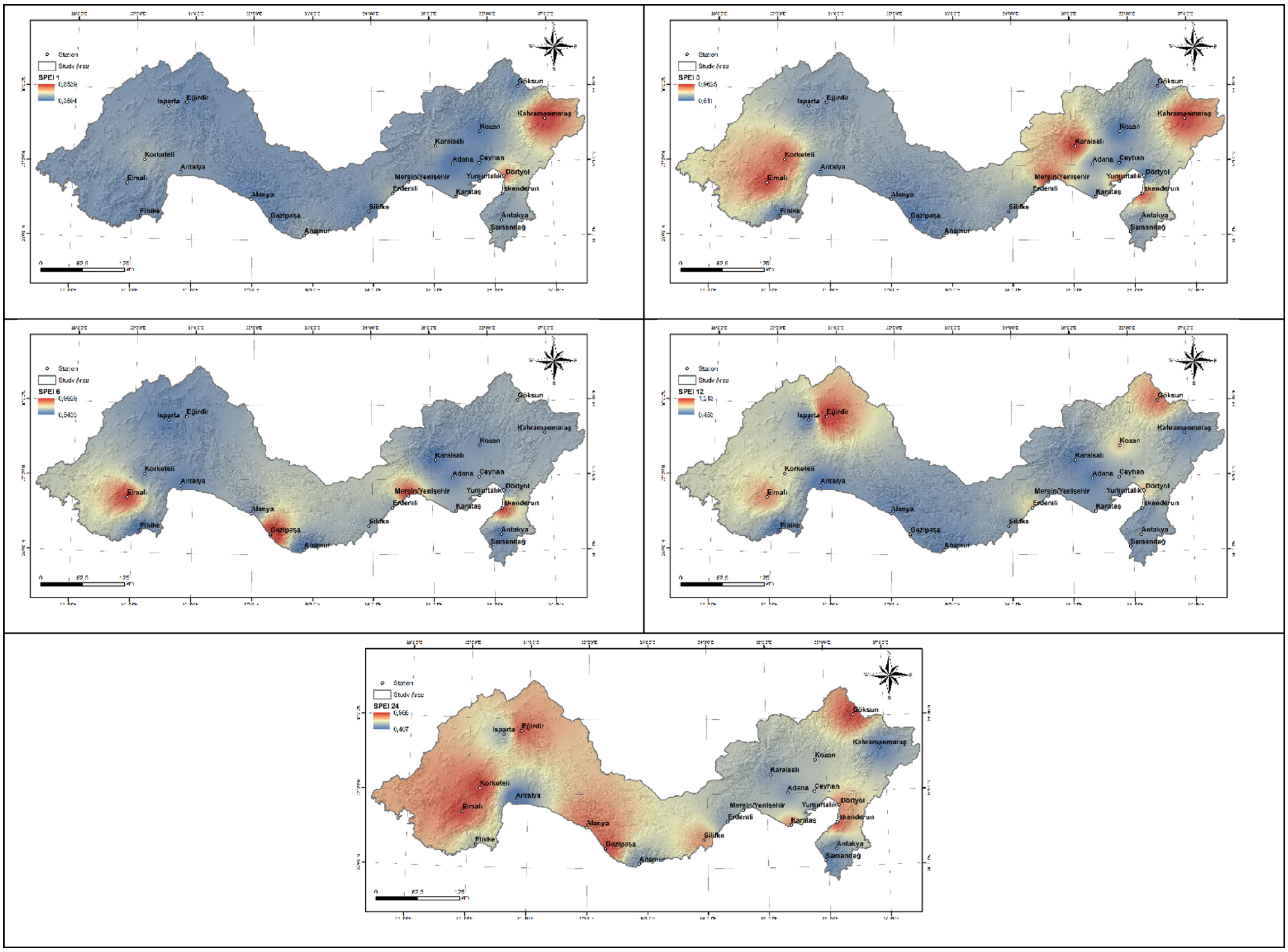

Fig. 5 Spatial variability of scaling exponents of SPEI series of the Mediterranean region at different time scales (1, 3, 6, 12 and 24 months)

and means large fluctuations are more frequent than small ones. It means that the severe or sudden changes in drought conditions have a greater influence on the multifractality of the drought in the region. The asymmetry index (r) further suggests that SPEI exhibits a more pronounced imbalance between extreme and moderate fluctuations, highlighting enhanced sensitivity to prolonged and intense drought conditions. Similarly, the width of the multifractal spectrum (W) is in general broader for SPEI, indicating increased intermittency and a wider range of scaling exponents, while the Hölder exponent ($\alpha 0$) points to shifts in the dominant scaling regime between SPI and SPEI. The deviation in the estimates are the least for $\alpha 0$ followed by W and highest for r for both SPI and SPEI series, irrespective of the time scale. Together, these results emphasize that SPEI captures a higher level of complexity and nonlinearity than SPI, underscoring the importance of incorporating evapotranspiration effects when assessing drought variability under climate change.

4.3 UDVG-based analysis and implications

In this exercise, the UDVG framework is invoked for the multifractal description of SPI and SPEI series, which enabled a comparison between the two schemes and their applicability. The key multifractal properties are determined upon UDVG analysis upon the inverted drought series of 3, 6 and 12-month drought representing short, moderate and long-term drought. The Renyi exponent plots (upper panels) and multifractal spectrum (lower panels) of SPI and SPEI series of Yumurtalık station, which is the most drought-prone location within the Mediterranean terrain, at different time scales, developed in a UDVG frame, are shown in Fig. 7, while similar plots of remaining six stations as representatives of three sub basins of the region are provided in SI file (Figure S7- Figure S12). The seven multifractal exponents were computed for each SPI and SPEI series of various stations at all the three-time scales using VG and UDVG methods, the complete values of which are provided in SI file (Table S2 and Tables S3). The non-parametric Kernel density estimator (KDE) and box plots are used to

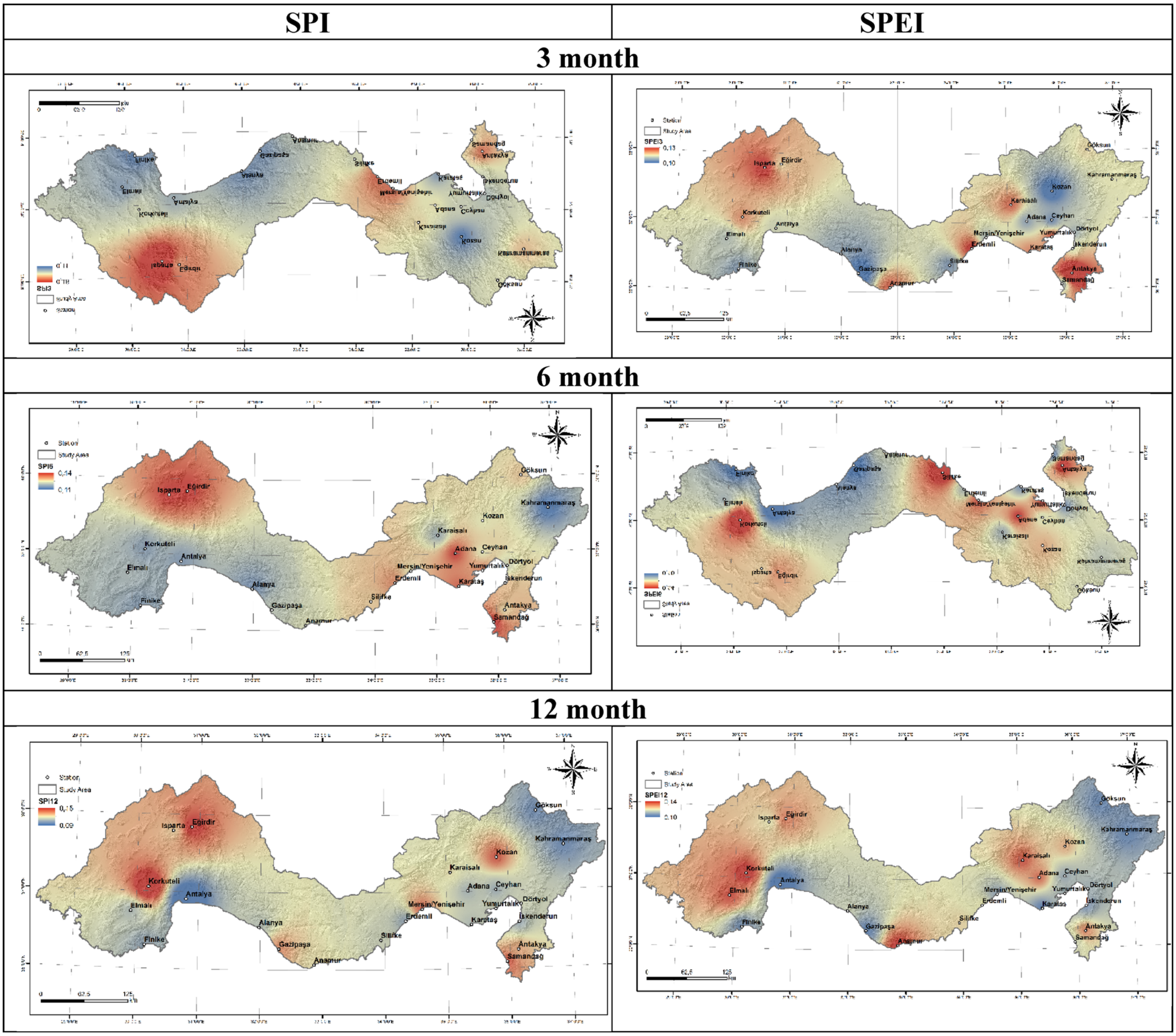

Fig. 6 Multifractality coefficient for SPI and SPEI series of the Mediterranean region at different time scales

illustrate and compare the variations. KDE based CDF of the parameters, to enable a comparison of the exponents of SPEI with that of SPI upon a UDVG frame, which is presented in Fig. 8. In Fig. 8, upper row shows the results of a 3-month series, the middle row shows the results of a 6-month series, and the lower row shows the results of a 12-month series.

The application of the UDVG method to drought indices such as the SPI and the SPEI reveals valuable information that the classical VG approach tends to overlook. Specifically, the UDVG enhances the detection of low-amplitude fluctuations, those associated with persistent, moderate droughts rather than extreme events.

Figure 7 shows that larger exponents for SPEI over SPI upon UDVG-based analysis. This is particularly relevant for SPEI, where the inclusion of evapotranspiration induces subtler temporal dynamics. Similar observations are made on considering the CDFs of the parameters presented in Fig. 8. Box plots of the seven multifractal parameters are presented in Fig. 9. In Fig. 9, D_0 denotes the fractal dimension, D_1 the correlation dimension, and D_2 the information entropy. The parameter Dq represents the generalized dimensions characterizing multifractal behavior, r is the asymmetry index, W denotes the width of the multifractal spectrum, and α corresponds to the Hölder exponent. The labels V and U refer to the VG-based and UDVG-based analyses, respectively.

The multifractal analysis conducted across 20 stations yields several key insights:

Table 4 Basic statistics of complementary multifractal parameters of SPI and SPEI, derived by VG method

Statistical Properties	Complementary multifractal properties					
	r	W	α0	*r*	W	α0
	SPI-3			SPEI-3		
Maximum	1.415	1.202	1.065	1.250	1.073	1.057
Minimum	0.768	0.840	0.986	0.800	0.793	0.989
Mean	1.066	0.970	1.026	0.967	0.882	1.023
Standard Deviation	0.166	0.099	0.025	0.121	0.058	0.020
	SPI-6			SPEI-6		
Maximum	1.538	1.121	1.05	1.750	1.093	1.014
Minimum	0.98	0.833	0.887	0.904	0.803	0.914
Mean	1.192	0.981	0.971	1.180	0.942	0.976
Standard Deviation	0.162	0.081	0.032	0.189	0.079	0.024
	SPI-12			SPEI-12		
Maximum	1.829	1.146	1.007	1.912	1.116	1.008
Minimum	1.020	0.811	0.848	0.980	0.811	0.873
Mean	1.261	0.945	0.908	1.283	0.922	0.925
Standard Deviation	0.196	0.085	0.036	0.215	0.086	0.035

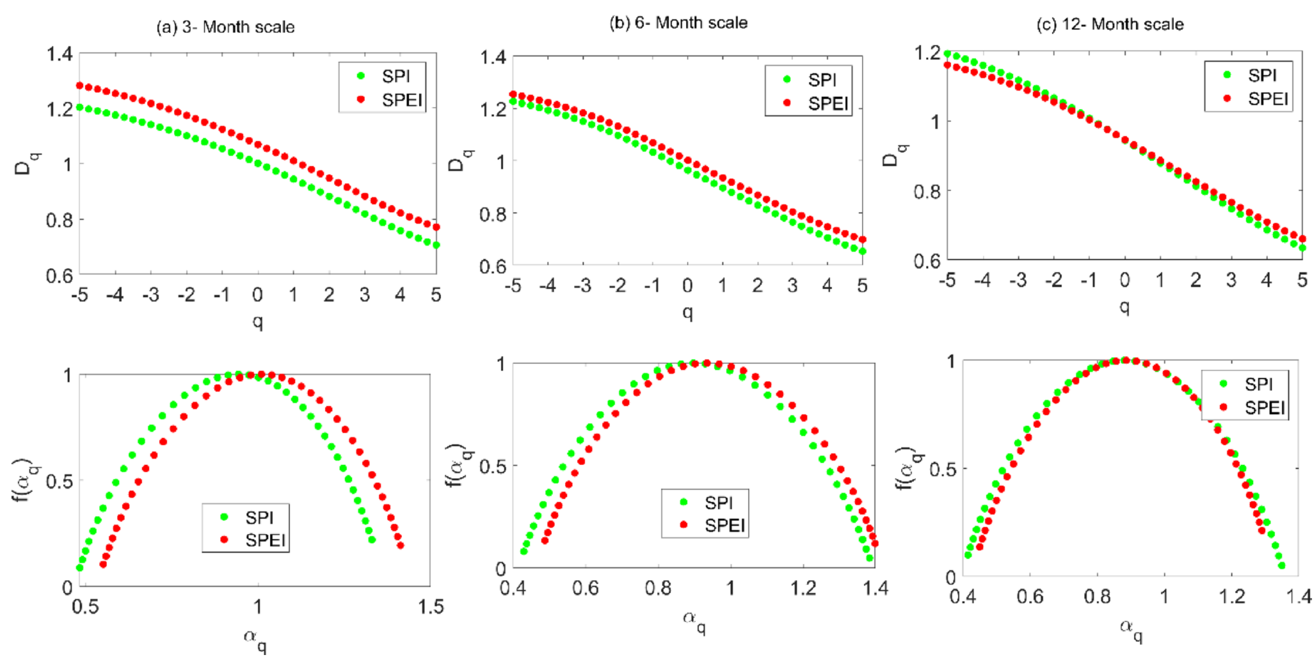

Fig. 7 Upside-down visibility graph based Renyi exponent plots (upper panels) and multifractal spectrum (lower panels) of SPI and SPEI series of Yumurtalık station at different time scales

- Reduced multifractal width (ΔDq) at shorter time scales: At the 6-month aggregation scale, the degree of multifractality ($\Delta Dq = D_0 - D_2$) derived from UDVG ranges from 0.36 to 0.62, with a mean value of 0.49 ± 0.07. In contrast, the VG method gives a significantly higher range of 0.48 to 0.95 (mean 0.72 ± 0.12). This consistent reduction in ΔDq, approximately 30% lower with UDVG, indicates that UDVG captures fewer high-amplitude fluctuations, focusing instead on the background variability of the signal.
- High temporal stability at longer scales: When the aggregation period increases to 24 months, the multifractality in UDVG remains stable (mean $\Delta Dq = 0.47 \pm 0.06$), whereas the VG-derived values increase considerably (mean $\Delta Dq = 0.81 \pm 0.15$). This suggests that the UDVG is less sensitive to time scale variations and better suited for representing long-term drought persistence.

Fig. 8 Comparison of CDFs of key multifractal properties of SPI and SPEI series of the Mediterranean region based on UDVG analysis

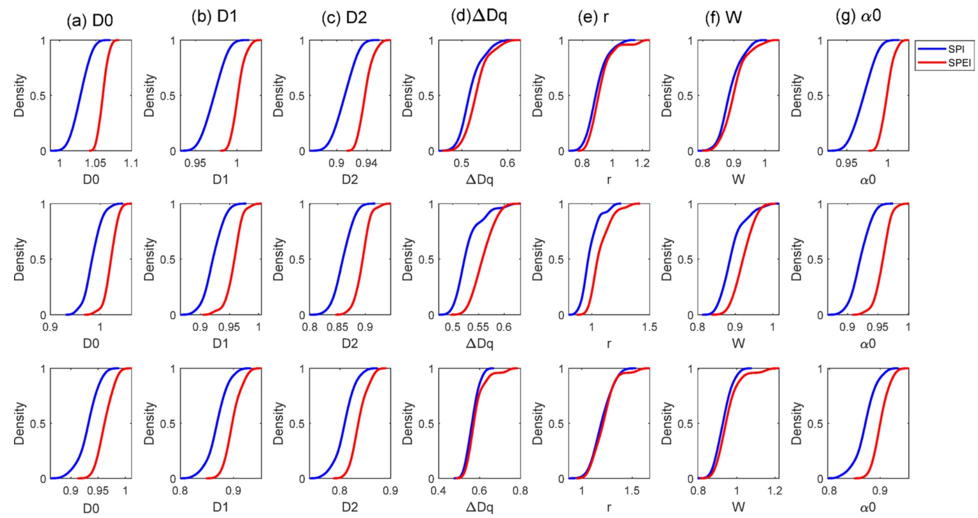

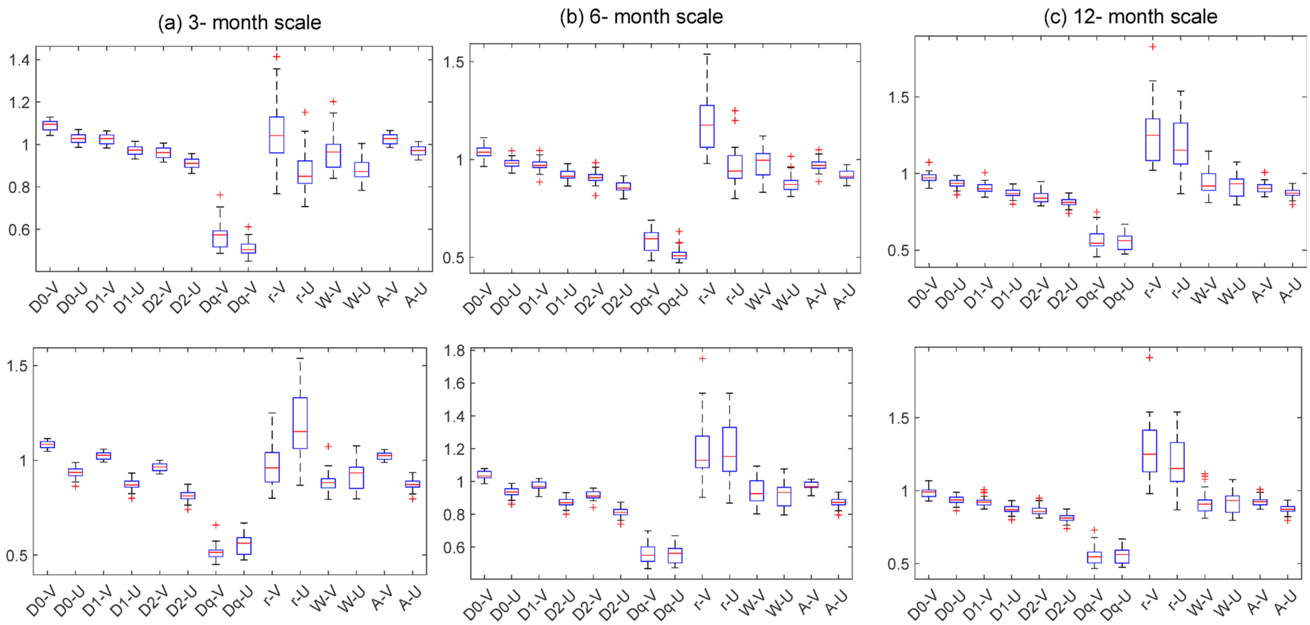

Fig. 9 Box plots of multifractal exponents of SPI (upper panels) and SPEI (lower panels) of different time scales

- Lower scaling exponent (λ) in UDVG: For SPI at a 12-month scale, the UDVG produces a mean scaling exponent λ of 1.02 (range: 0.85–1.18), compared to 1.15 (range: 1.01–1.34) for VG. A lower λ implies a heavier tail in the node degree distribution for low-degree nodes, consistent with an emphasis on small, frequent drought deviations.
- Greater sensitivity to evapotranspiration dynamics: The difference in multifractal width between VG and UDVG is more pronounced for SPEI than for SPI. On average, the reduction in ΔDq when switching from VG to UDVG is 0.29 for SPEI versus 0.21 for SPI. This suggests that SPEI, by incorporating temperature and evapotranspiration effects, contains more low-amplitude variability, which is precisely the type of signal that UDVG is best equipped to detect.

The critical analysis of Fig. 9 shows that on considering the SPI series, the VG based estimates are giving higher median values over its UD counterpart except for the multifractal width and spread of 12-month time scale. One can see that similar larger median estimates of UDVG over VG for SPEI series, irrespective of time scales. This basically depends upon the density (number) of wet and drought events prominent in the region. The dominancy of prolonged long-term dry events in the region will be influenced by inversion of the series upon a UG analysis. The difference between VG and UDVG was more pronounced in SPEI, confirming the role of temperature-driven evapotranspiration in modulating drought signal variability. In short, the UDVG approach yielded lower ΔDq values, pointing to smoother, more persistent fluctuations. Across all stations, the singularity spectra f(α) for SPI demonstrated wider support in VG than in UDVG, further supporting the hypothesis that UDVG is more sensitive to low-intensity variations, thereby characterizing the background drought regime.

5 Discussion

SPI is a widely used indicator of precipitation deficit or surplus for drought monitoring. However, precipitation and drought processes are inherently nonlinear and scale-dependent, meaning that classical linear statistics (e.g., mean, variance, correlation) often fail to capture their full dynamics. In this context, multifractal analysis provides a powerful framework to quantify how drought variability and persistence evolve across temporal scales, allowing SPI and SPEI to exhibit distinct behaviours at short (monthly) versus long (seasonal to multi-year) timescales. SPI fluctuations are irregular and intermittent, and multifractal analysis quantifies both the intensity and heterogeneity of these fluctuations, revealing clustering of dry and wet periods as well as long-range dependence. Such properties are directly linked to the physical persistence of droughts and their potential predictability limits, which are crucial for water resources, agriculture, and risk management.

Multifractality in hydrological and drought processes arises from two primary physical mechanisms. First, climate and precipitation are influenced by persistent atmospheric circulation patterns, large-scale climatic oscillations (e.g., El Niño–Southern Oscillation), and land-atmosphere feedbacks, which introduce long-range correlations into SPI and SPEI time series. Second, precipitation extremes, although relatively rare, produce strong non-Gaussian behaviour, and their occurrence across multiple temporal scales leads to multifractal structures. Short-term variability is mainly driven by local weather and storm clustering, whereas long-term variability reflects large-scale climatic controls, and their interaction generates the observed multifractal behaviour in drought indices.

The main novelty of this study lies in the application of a dual visibility-graph framework (VG and UDVG) to investigate the multifractal structure of SPI and SPEI time series. Unlike traditional multifractal techniques such as box-counting or detrended fluctuation analysis, the visibility graph approach maps the temporal structure of drought indices into complex networks, enabling the extraction of physically interpretable network-based scaling exponents. This allows us to explicitly distinguish between high-amplitude (wet or excess rainfall) events and low-amplitude, persistent drought fluctuations within the same analytical framework. Fractal dimension and hence Hurst exponent can tell persistence/anti-persistence is uniform across fluctuation magnitudes. Spectrum can measure the richness of scaling, like wide spectrum implies more complexity and droughts are highly intermittent, extremes dominate, harder to forecast. Degree of multifractality quantifies how strongly drought/wet extremes differ from average conditions and if it is less droughts/wets are more uniform, easier to predict.

Previous studies have highlighted the relevance of multifractal approaches for understanding hydrological and drought-related processes. For instance, Adarsh et al. (2019) demonstrated that multifractal analysis captures the scale-dependent persistence and complexity of drought indices. The generalized dimensions Dq characterize scaling heterogeneity and confirm that drought dynamics deviate from monofractal behaviour. The width of the multifractal spectrum (W) reflects the range of singularities and thus the degree of intermittency, while the asymmetry index (r) reveals imbalances between large and small fluctuations, indicating preferential clustering of specific drought intensities. The Hölder exponent (α0) identifies the dominant scaling regime of the process. Together, these parameters link the mathematical description of multifractality to physically meaningful drought characteristics such as persistence, intermittency, and asymmetry between wet and dry conditions (Hou et al. 2018; Adarsh et al. 2019). Our results are fully consistent with these findings and further extend them by introducing a dual VG–UDVG framework that explicitly separates wet and dry regimes, thereby enhancing the physical interpretation of SPI and SPEI dynamics across temporal scales. Some of the studies on PM_{10} time series highlighted the relevance and effectiveness of combining VG and UDVG methods within a multifractal analysis framework to distinguish between high and low fluctuation regimes in environmental data (Plocoste et al. 2021b). This dual-network approach revealed that UDVG is particularly suited to capturing low-intensity background dynamics, a crucial aspect when studying phenomena such as chronic pollution exposure or, in the case of drought indices, persistent but moderate deficits in precipitation. Applying this methodology to SPI and SPEI indices—datasets known for their stochastic nature and complex temporal behavior—can provide valuable insights into the multiscale structure of drought dynamics, especially in discriminating between short-term variability and long-term persistence.

The proposed framework also provides many exponents (D_0 or box-counting dimension, D_1 or information entropy, D_2 or correlation dimension, as stated earlier). Lesser (D_0 - D_1) depict that the series is more regular. The value of D2 is helpful to determine the recurrence and if (D_0-D_2), i.e., the chances of repeating the same value will be more. The proposed VGMF framework integrates multitude of mathematical techniques for multifractal description, as also demonstrated in our earlier work on river flow (Shamseena and Adarsh 2025). In air pollution studies, it was reported that the multifractal degree () is higher for VG than UDVG (Plocoste et al. 2021b), which not necessarily universal, as shown for hydrologic index datasets of different character as noted in this study. VG and UDVG rely on the *relative shape* of the signal, not on the sign of the values. VG is constructed based on geometric visibility between points in the time series. Whether the values are positive or negative does not affect the ability to build a meaningful network — what matters is the temporal structure of the data. The UDVG approach is particularly suitable for SPI/SPEI, as the VG emphasizes positive spikes, i.e., *wet periods* or excess rainfall, while UDVG brings out *dry periods* (negative SPI/SPEI), making it especially useful for analyzing drought behavior. Hubs in UDVG correspond to intense or persistent drought events, not wet anomalies. The symmetry of SPI/SPEI around zero actually makes them ideal candidates for joint VG/UDVG analysis, capturing both wet and dry extremes.

A key finding of this study is that the VG and UDVG methods provide complementary but distinct perspectives on drought behaviour. VG is primarily sensitive to positive excursions in SPI and SPEI, corresponding to wet periods or excess precipitation, whereas UDVG highlights negative excursions, i.e., drought conditions. Because SPI and SPEI are standardized and symmetric around zero, they are particularly well suited for a joint VG/UDVG analysis, which captures both wet and dry extremes as well as persistent background droughts. In the UDVG representation, network hubs correspond to intense or long-lasting drought events rather than wet anomalies, providing a physically intuitive interpretation of drought persistence. From an operational perspective, this dual-network framework has important implications for drought monitoring and early warning. While extreme droughts are often the focus of risk assessments, low-amplitude and persistent rainfall deficits can act as early indicators of slowly developing agricultural or hydrological droughts. Detecting such subtle changes is critical for proactive water management and disaster preparedness. The UDVG approach enhances the ability to detect these precursory signals, complementing traditional drought indices and offering a more nuanced understanding of drought evolution under changing climatic conditions. Further multifractal models can be developed as alternative pathways for forecasting of drought indicators, which may help us in developing early warning systems of droughts. It can assist decision-makers in identifying gradual, cumulative drought risks, often precursors to major drought episodes, and in refining early warning systems and long-term adaptation policies.

This paper uniquely applied visibility graph approach and its upside-down variant for analyzing the multifractality of the drought considering the SPI and SPEI time series. On comparing within traditional approaches, the low amplitude fluctuations in drought indices can also be captured satisfactorily well using the UDVG variant of visibility graph. Here VG and UDVG provides additional indices like information entropy, correlation dimension etc. along with fractal dimension, which may help in assessing the complexity of the series (Rajesh et al. 2025), while from other classical methods like box counting or detrending methods like MFDFA such information is not directly deduced. Even though the large-scale droughts are predicatively important, the low amplitude fluctuations are cautionary sign, lead to long term drought small changes can be early indicators of significant, slow-developing disasters. Hence detecting subtle, low-amplitude changes in drought indicators helps in developing early warning, response cum disaster preparedness. Moreover, one type of drought may lead to other droughts, like propagation. For example, reduction in rainfall and small changes can make an impact on soil moisture and eventually can impact the agricultural sector and water resource management. Hence identification of early detection of low-amplitude rainfall deficit may be a warning for the possible agricultural or hydrological droughts in the months ahead. In such a scenario, UDVG approach can offer more credible characterization of standardized indices, which eventually help in developing early warning system for meteorological drought, getting prepared against possible hydrological or agricultural drought.

Multifractal analysis can quantify the ranges SPI signals often show scale invariance (self-similarity). The drought indices like SPI can be predicted in advance using machine learning models or its hybrid decomposition variants (Adarsh and Janga Reddy 2019; Alkubaisi et al. 2025). The magnitudes can further be used to quantify the state like severe, extreme or moderate drought and the risk assessment can be made. Moreover, drought risk can be estimated and hazard assessment can be made using appropriate diverse statistical tools including copulas (Reddy and Ganguly 2012; Adarsh et al. 2018; Ganjir et al. 2025) Strong multifractality suggests that extreme drought/wet events may likely be unpredictable. However, such information is useful for water resources, agriculture, and hazard planning and risk assessment. Along with the high magnitude fluctuations, the low magnitude indices are also important as it can be early indicator of a possible drought episode of future or even the transition of meteorological to hydrological drought.

Finally, this study opens new avenues for future research. The proposed VG–UDVG multifractal framework can be extended to other drought indices (e.g., reconnaissance drought index, soil moisture deficit index, streamflow drought indices, normalized difference vegetation index) and to non-stationary hydrological variables such as soil moisture and river discharge. Further exploration of alternative visibility graph schemes may also improve the characterization of drought dynamics in time series containing both positive and negative fluctuations.

6 Conclusions

This study proposed a novel visibility graph framework for the multifractal description of drought by demonstrating the applicability of SPI and SPEI series of the Mediterranean region at diverse drought scales. The important conclusions include:

- All the time series of SPI and SPEI series of the region and stochastic origin, except for the immediate 1-month time series of a few stations. For the same station, both SPI and SPEI need not be chaotic, which implies the definite role of evapotranspiration in fluctuations.
- Short-term drought series are more complex than long-term drought, but the dominance of wet-dry time spells is critical in describing the multifractal features of the series.
- VG and UDVG-based frameworks are efficient in describing the drought dynamics. VG is especially used for analyzing the peaks (wet conditions) and it is useful for system response to excess water, UDVG is useful for analyzing the behaviour during drought periods, i.e. valleys (dry conditions).
- SPEI is more complex than the SPI series, especially when evapotranspiration plays a major role along with precipitation in describing the drought conditions. In such cases, UDVG analysis possesses a certain definite advantage in revealing the complexity of drought dynamics.

Supplementary Information The online version contains supplementary material available at https://doi.org/10.1007/s00477-026-03176-4.

Author contributions TP and AS conceptualized the work. OS and UZ collected and processed the data. TP improved the code and AS performed the analysis. OS and UZ made visualization. OS, AS and TP interpreted the results. OS and AS prepared the draft version of the manuscript. AS and TP prepared the present version and all authors approved this version.

Funding No funding received to perform this research work.

Data availability All the data used in the study will be shared upon reasonable request made to the corresponding author.

Declarations

Competing interests The authors declare no competing interests.

Informed consent Not applicable.

Institutional review board Not applicable.

References

Achite M, Simsek O, Sankaran A, Katipoğlu OM, Caloiero T (2024) Analyzing the dynamical relationships between meteorological and hydrological drought of Wadi Mina basin, Algeria using a novel multiscale framework. Stoch Env Res Risk Assess 38(5):1935–1953

Adarsh S, Janga Reddy M (2019) Evaluation of trends and predictability of short-term droughts in three meteorological subdivisions of India using multivariate EMD-based hybrid modelling. Hydrol Process 33(1):130–143

Adarsh S, Karthik S, Shyma M, Prem GD, Parveen S, A. T., Sruthi N (2018) Developing short-term drought severity-duration-frequency curves for Kerala meteorological subdivision, India, using bivariate copulas. KSCE J Civ Eng 22(3):962–973

Adarsh S, Kumar DN, Deepthi B, Gayathri G, Aswathy SS, Bhagyasree S (2019) Multifractal characterization of meteorological drought in India using detrended fluctuation analysis. Int J Climatol. 39:4234–4255. https://doi.org/10.1002/joc.6070

Alkubaisi H, Danandeh Mehr A, S, A., Khan MMH (2025) Drought modelling and forecasting using shallow and deep machine learning techniques. Model Earth Syst Environ 11(1):41 , https://doi.org/10.1007/s40808-024-02268-w

Azizi H, Sulaimany S (2024) A review of visibility graph analysis. IEEE Access 12:93517–93530. https://doi.org/10.1109/ACCESS.2024.3401485

Azizi S, Azizi T (2022) The fractal nature of drought: power laws and fractal complexity of Arizona drought. Eur J Math Anal 2:17–17. https://doi.org/10.28924/ada/ma.2.17

Azizi S, Azizi T (2024) Classification of drought severity in contiguous USA during the past 21 years using fractal geometry. EURASIP J Adv Signal Process 3(2024). https://doi.org/10.1186/s13634-023-01094-z

Bassingthwaighte JB, Raymond GM (1994) Evaluating rescaled range analysis for time series. Ann Biomed Eng 22:432–444. https://doi.org/10.1007/BF02368250

Braga AC, Alves LGA, Costa LS, Ribeiro AA, De Jesus MMA, Tateishi AA (2016) Characterization of river flow fluctuations via horizontal visibility graphs. Phys Stat Mech Appl 444:1003–1011. https://doi.org/10.1016/j.physa.2015.10.102

Burrough PA (1986) Principles of geographical information systems for land resources assessment. Geocarto Int 1(3):54. https://doi.org/10.1080/10106048609354060

Carmona-Cabezas R, Ana B, Ariza-Villaverde FJ, Jiménez-Hornero (2019) Visibility graphs of ground-level ozone time series: a multifractal analysis. Sci Total Environ 661:138–147. https://doi.org/10.1016/j.scitotenv.2019.01.147

Carmona-Cabezas R, Gómez-Gómez J, Gutiérrez de Ravé E, Sánchez-López E, Serrano J, Jiménez-Hornero FJ (2020) Improving graph-based detection of singular events for photochemical smog agents. Chemosphere 253:126660 , https://doi.org/10.1016/j.chemosphere.2020.126660

Chen H, Sun J (2017) Characterizing present and future drought changes over Eastern China. Int J Climatol 37:138–156. https://doi.org/10.1002/joc.4987

Chhabra AB, Jensen RV, Sreenivasan KR (1989) Extraction of underlying multiplicative processes from multifractals via the thermodynamic formalism. Phys Rev A 40(8):4593

da Silva ASA, Stosic T, Arsenić I, Menezes RSC, Stosic B (2023) Multifractal analysis of standardized precipitation index in Northeast Brazil. Chaos Solitons Fractals 172:113600 , https://doi.org/10.1016/j.chaos.2023.113600

De Bartolo SG, Gaudio R, Gabriele S (2004) Multifractal analysis of river networks: sandbox approach. Water Resour Res 40(2) https://doi.org/10.1029/2003WR002760

Deepthi B, Sivakumar B (2023) Towards assessing the importance of individual stations in hydrometric networks: application of complex networks. Stoch Env Res Risk Assess 37(4):1333–1352

Dibike Y, Prowse T, Bonsal B, O'Neil H (2017) Implications of future climate on water availability in the Western Canadian river basins. Int J Climatol 37(7):3247–3263. https://doi.org/10.1002/joc.4912

Feng S, Trnka M, Hayes M, Zhang Y, Feng S, Trnka M, Hayes M, Zhang Y (2017) Why do different drought indices show distinct future drought risk outcomes in the U.S. Great plains? J Clim 30(1):265–278. https://doi.org/10.1175/JCLI-D-15-0590.1

Ganjir G, Reddy MJ, Karmakar S (2025) Assessing agricultural drought hazard, vulnerability and risk over India. Int J Disaster Risk Reduct 130:105830. https://doi.org/10.1016/j.ijdrr.2025.105830

Gao X, Zhao Q, Zhao X, Wu P, Pan W, Gao X, Sun M (2017) Temporal and Spatial evolution of the standardized precipitation evapotranspiration index (SPEI) in the loess plateau under climate change from 2001 to 2050. Sci Total Environ 595:191–200. https://doi.org/10.1016/J.SCITOTENV.2017.03.226

Ghimire GR, Jadidoleslam N, Krajewski WF, Tsonis AA (2020) Insights on streamflow predictability across scales using horizontal visibility graph based networks. Front Water 2:17. https://doi.org/10.3389/frwa.2020.00017

Giorgi F, Lionello P (2008) Climate change projections for the mediterranean region. Glob Planet Chang 63(2–3):90–104. https://doi.org/10.1016/j.gloplacha.2007.09.005

Gu L, Jamshidi S, Zhang M, Gu X, Wang Z (2024) Multifractal description of the agricultural and meteorological drought propagation process. Water Resour Manag 38(10):3607–3622

Gumus V, Simsek O, Avsaroglu Y, Agun B (2021) Spatio-temporal trend analysis of drought in the GAP Region, Turkey. Nat Hazards 109(2):1759–1776. https://doi.org/10.1007/s11069-021-04897-1

Habib A (2020) Exploring the physical interpretation of long-term memory in hydrology. Stoch Environ Res Risk Assess 34(12):2083–2091

Habib A, Butler AP, Bloomfield JP, Sorensen JPR (2022) Fractal domain refinement of models simulating hydrological time series. Hydrol Sci J 67(9):1342–1355. https://doi.org/10.1080/02626667.2022.2084342

Hayes M, Svoboda M, Wall N, Widhalm M (2011) The Lincoln declaration on drought indices: universal meteorological drought index recommended. Bull Am Meteorol Soc 92(4):485–488. https://doi.org/10.1175/2010BAMS3103.1

Hou W, Feng G, Yan P et al (2018) Multifractal analysis of the drought area in seven large regions of China from 1961 to 2012. Meteorol Atmos Phys 130:459–471. https://doi.org/10.1007/s00703-017-0530-0

Hurst HE (1951) Long-term storage capacity of reservoirs. Trans Am Soc Civil Eng 116(1):770–799

Isaaks EH, Srivastava RH (1989) An introduction to applied geostatistics. Oxford University Press, New York

Kantelhardt JW, Koscielny-Bunde E, Rybski D, Braun P, Bunde A, Havlin S (2006) Long-term persistence and multifractality of precipitation and river runoff records. J Geophys Res Atmos 111(D1). https://doi.org/10.1029/2005JD005881

Kantelhardt JW, Zschiegner SA, Koscielny-Bunde E, Halvin S, Bunde A, Stanley H (2002) Multifractal detrended fluctuation analysis of non-stationary time series. Phys Stat Mech Appl 316:87–114

Keskiner AD, Simsek O (2024) Evaluation of the sensitivity of meteorological drought in the mediterranean region to different data record lengths. Environ Monit Assess 196(7):602. https://doi.org/10.1007/s10661-024-12726-8

Lacasa LA, Nuñez E, Roldán JMR, Parrondo, Luque B (2012) Time series irreversibility: a visibility graph approach. Eur Phys J B 85, 217 (2012). https://doi.org/10.1140/epjb/e2012-20809-8

Lacasa L, Luque B, Ballesteros F, Luque J, Nuno JC (2008) From time series to complex networks: the visibility graph. Proc Natl Acad Sci 105(13):4972–4975

Lacasa L, Luque B, Luque J, Nuno JC (2009) The visibility graph: A new method for estimating the Hurst exponent of fractional brownian motion. Europhys Lett 86(3):30001

Lacasa L, Toral R (2010) Description of stochastic and chaotic series using visibility graphs. Phys Rev E Stat Nonlinear Soft Matter Phys 82(3):036120

Lionello P, Malanotte-Rizzoli P, Boscolo R, Alpert P, Artale V, Li L, Luterbacher J, May W, Trigo R, Tsimplis M, Ulbrich U, Xoplaki E (2006) The mediterranean climate: an overview of the main characteristics and issues. Dev Earth Environ Sci 4:1–26. https://doi.org/10.1016/S1571-9197(06)80003-0

Luque BL, Lacasa F, Ballesteros J, Luque (2009) Horizontal visibility graphs: exact results for random time series. Phys Rev E 80:103. https://doi.org/10.1103/PhysRevE.80.046103

Mandelbrot B (1989) Fractal geometry: what is it, and what does it do? Proc R Soc Lond A 4233–16. https://doi.org/10.1098/rspa.1989.0038

Mandelbrot BB (1971) A fast fractional Gaussian noise generator. Water Resour Res 7(3):543–553. https://doi.org/10.1029/WR007i003p00543

Mandelbrot BB (1983) The fractal geometry of nature/Revised and enlarged edition. New York

Mandelbrot BB, Wallis JR (1969) Some long-run properties of geophysical records. Water Resour Res 5(2):321–340. https://doi.org/10.1029/WR005i002p00321

McKee TB, Doesken NJ, Kleist J (1993) The relationship of drought frequency and duration to time scales. In: Proceedings of the 8th conference on applied climatology, Anaheim, CA, USA, 17–22 January ; Volume 17, pp 179–183

Mishra AK, Singh VP (2010) A review of drought concepts. J Hydrol 391(1–2):202–216

NRC (1991) Opportunities in the hydrologic sciences. National Academies, Washington, DC

Pachore A, Bajirao R, Remesan, Rohini K (2024) Multifractal characterization of meteorological to agricultural drought propagation over India. Sci Rep 14(1):18889 https://doi.org/10.1038/s41598-024-68534-0

Peng CK, Buldyrev SV, Simons M, Stanley HE, Goldberger AL (1994) Mosaic organization of DNA nucleotides. Phys Rev E 49:1685–1689

Plocoste T, Carmona-Cabezas R, Jiménez-Hornero FJ, de Gutiérrez E (2021b) Background PM10 atmosphere: in the seek of a multifractal characterization using complex networks. J Aerosol Sci 155:105777. https://doi.org/10.1016/j.jaerosci.2021.105777

Plocoste T, Carmona-Cabezas R, Jiménez-Hornero FJ, Gutiérrez de Ravé E, Calif R (2021a) Multifractal characterisation of particulate matter (PM10) time series in the Caribbean basin using visibility graphs. Atmos Pollut Res 12(1):100–110. https://doi.org/10.1016/j.apr.2020.08.027

Rahmani F, Fattahi MH (2021) A multifractal cross-correlation investigation into sensitivity and dependence of meteorological and hydrological droughts on precipitation and temperature. Nat Hazards 109(3):2197–2219

Rahmani F, Fattahi;, MH (2024) Exploring the sensitivity of river flow patterns to meteorological drought using multifractal and cross-correlation applications. J Water Clim Chang 15(8):4127–4137. https://doi.org/10.2166/wcc.2024.310

Rajesh SM, Santhoshkhan S, Muraleekrishnan B, Adarsh S (2025) Analyzing the streamflow-suspended sediment synchronization across major Indian river basins using cross recurrence analysis. J Hydrol 134587 https://doi.org/10.1016/j.jhydrol.2025.134587

Rangarajan G, Sant DA (1997) A climate predictability index and its applications. Geophys Res Lett 24(10):1239–1242

Rangarajan G, Sant DA (2004) Fractal dimensional analysis of Indian Climatic dynamics. Chaos Solitons Fractals 19(2):285–291

Reddy MJ, Ganguli P (2012) Application of copulas for derivation of drought severity–duration–frequency curves. Hydrol Process 26(11):1672–1685

Salvacion AR (2021) Mapping meteorological drought hazard in the Philippines using SPI and SPEI. Spat Inf Res 29:949–960. https://doi.org/10.1007/s41324-021-00402-9

Schertzer D, Lovejoy S (1987) Physical modeling and analysis of rain and clouds by anisotropic scaling multiplicative processes. J Geophys Res Atmos 92(D8):9693–9714

Shamseena V, Adarsh S (2025) Multifractal applications in hydro-climatology: a comprehensive review of modern methods. Fractal Fract. 9(1):27. https://doi.org/10.3390/fractalfract9010027

Shamseena V, Alikkal S, Kunnummal SJ et al (2025) Fractal complexity evaluation for the predictability assessment of daily streamflows of Indian river basins. Eur Phys J Spec Top (2025). https://doi.org/10.1140/epjs/s11734-025-01636-6

Shang P, Kame S (2005) Fractal nature of time series in the sediment transport phenomenon. Chaos Solitons Fractals 26:997–1007

Shepard D (1968) A two-dimensional interpolation function for irregularly-spaced data. ACM '68: Proc 1968 23rd ACM Natl Conf 517–524. https://doi.org/10.1145/800186.810616

Simsek O (2021) Hydrological drought analysis of mediterranean basins, Turkey. Arab J Geosci 14(20):2136. https://doi.org/10.1007/s12517-021-08501-5

Simsek O, Şenol Hİ, Keskiner AD (2025) Examination of area-based trend and drought characteristics of drought classes in the context of climate change. Nat Hazards 1–26. https://doi.org/10.1007/s11069-025-07412-y

Singh GR, Jain MK, Gupta V (2019) Spatiotemporal assessment of drought hazard, vulnerability and risk in the Krishna River basin, India. Nat Hazards 99:611–635. https://doi.org/10.1007/s11069-019-03762-6

Sivakumar B, &Woldemeskel FM (2014) Complex networks for streamflow dynamics. Hydrol Earth Syst Sci 18(11):4565–4578

Spinoni J, Vogt JV, Naumann G, Barbosa P, Dosio A (2018) Will drought events become more frequent and severe in Europe? Int J Climatol 38(4):1718–1736. https://doi.org/10.1002/joc.5291

Svoboda MD, Fuchs BA (2016) Handbook of drought indicators and indices, vol 2. World Meteorological Organization Geneva, Switzerland

Tatli H, Dalfes HN (2020) Long-time memory in drought via detrended fluctuation analysis. Water Resour Manag 34(3):1199–1212

Tatli T (2015) Detecting persistence of meteorological drought via Hurst exponent. Meteorol Appl 22:763–769. https://doi.org/10.1002/met.1519

Thomas T, Jaiswal RK, Nayak PC, Ghosh NC (2015) Comprehensive evaluation of the changing drought characteristics in Bundelkhand region of central India. Meteorol Atmos Phys 127(2):163–182

Thom HCS (1958) A note on the gamma distribution. Mon Weather Rev 86(4):117–122. https://doi.org/10.1175/1520-0493(1958)086%3C0117:ANOTGD%3E2.0.CO;2

Thornthwaite CW (1948) An approach toward a rational classification of climate. Geogr Rev 38:55–94. https://doi.org/10.2307/210739

Tirivarombo S, Osupile D, Eliasson P (2018) Drought monitoring and analysis: standardised precipitation evapotranspiration index (SPEI) and standardised precipitation index (SPI). Phys Chem Earth Parts A/B/C 106:1–10. https://doi.org/10.1016/j.pce.2018.07.001

Tél T, Fülöp Á, Vicsek T (1989) Determination of fractal dimensions for geometrical multifractals. Phys A 159:155–166

Vicente-Serrano S, Beguería S, López-Moreno JI (2010a) A multiscalar drought index sensitive to global warming: the standardized precipitation evapotranspiration index. J Clim 23:1696–1718. https://doi.org/10.1175/2009JCLI2909.1

Vicente-Serrano SM, Beguería S, López-Moreno JI, Angulo M, Kenawy E, A (2010b) A new global 0.5° gridded dataset (1901–2006) of a multiscalar drought index: comparison with current drought index datasets based on the Palmer drought severity index. J Hydrometeorol 11(4):1033–1043. https://doi.org/10.1175/2010JHM1224.1

Vicente-Serrano SM, Lopez-Moreno J-I, Beguería S, Lorenzo-Lacruz J, Sanchez–Lorenzo A, García-Ruiz JM, Azorin-Molina C, Morán-Tejeda E, Revuelto J, Trigo R, Coelho F, Espejo F (2014) Evidence of increasing drought severity caused by temperature rise in Southern Europe. Environ Res Lett 9(4):044001. https://doi.org/10.1088/1748-9326/9/4/044001

Vicsek T (1990) Mass multifractals. Physica A 168(1):490–497

Wu C, Xian Z, Huang G (2016) Meteorological drought in the Beijiang river basin, South china: current observations and future projections. Stoch Env Res Risk Assess 30(7):1821–1834. https://doi.org/10.1007/s00477-015-1157-7

Zargar A, Sadiq R, Naser B, Khan FI (2011) A review of drought indices. Environ Rev 19(NA):333–349

Zeybekoglu U, Sımsek O, Durgun EC (2025) Relationship between mediterranean region temperatures and precipitation with atmospheric oscillations and ITA results. J Coast Conserv 29:90. https://doi.org/10.1007/s11852-025-01173-3

Zhan C, Liang C, Zhao L, Jiang S, Niu K, Zhang Y (2023) Multifractal characteristics of multiscale drought in the yellow river Basin, China. Physica A 609:128305 , https://doi.org/10.1016/j.physa.2022.128305

Zhang Y, Yu Z, Niu H (2018) Standardized precipitation evapotranspiration index is highly correlated with total water storage over China under future climate scenarios. Atmos Environ 194:123–133. https://doi.org/10.1016/J.ATMOSENV.2018.09.028